

## RESEARCH ARTICLE

10.1002/2015JA022185

## Key Points:

- A 44 h prolonged southward IMF- $B_z$
- The draping of the radial field lines around the CMEs in the shocked plasma explains the polarity changes of the IMF- $B_z$  at 1 AU
- The solar wind density pulses show a distinct one-to-one correspondence with global geomagnetic response

## Correspondence to:

S. K. Bisoi,  
susanta@nao.cas.cn

## Citation:

Bisoi, S. K., D. Chakrabarty, P. Janardhan, R. G. Rastogi, A. Yoshikawa, K. Fujiki, M. Tokumaru, and Y. Yan (2016), The prolonged southward IMF- $B_z$  event of 2–4 May 1998: Solar, interplanetary causes and geomagnetic consequences, *J. Geophys. Res. Space Physics*, *121*, doi:10.1002/2015JA022185.

Received 19 NOV 2015

Accepted 14 APR 2016

Accepted article online 2 MAY 2016

## The prolonged southward IMF- $B_z$ event of 2–4 May 1998: Solar, interplanetary causes and geomagnetic consequences

Susanta Kumar Bisoi<sup>1</sup>, D. Chakrabarty<sup>2</sup>, P. Janardhan<sup>3</sup>, R. G. Rastogi<sup>4</sup>, A. Yoshikawa<sup>5</sup>, K. Fujiki<sup>6</sup>, M. Tokumaru<sup>6</sup>, and Y. Yan<sup>1</sup>

<sup>1</sup>Key Laboratory of Solar Activity, National Astronomical Observatories, Chinese Academy of Sciences, Beijing, China,

<sup>2</sup>Space and Atmospheric Sciences Division, Physical Research Laboratory, Ahmedabad, India, <sup>3</sup>Astronomy and Astrophysics Division, Physical Research Laboratory, Ahmedabad, India, <sup>4</sup>Physical Research Laboratory, Ahmedabad, India,

<sup>5</sup>Department of Earth and Planetary Sciences, International Center for Space Weather Science and Education, Kyushu University, Fukuoka, Japan, <sup>6</sup>Institute for Space-Earth Environmental Research, Nagoya University, Nagoya, Japan

**Abstract** A detailed investigation is carried out to understand the prolonged (~44 h) weakly southward interplanetary magnetic field (IMF- $B_z$ ) condition during 2–4 May 1998. In situ observations, during the period, show the passage of an expanding magnetic cloud embedded in an interplanetary coronal mass ejection (ICME), followed up by a shock and an interplanetary discontinuity driven by another ICME. It is the arrival of the ICMEs and the upfront shocks that caused the prolonged southward IMF- $B_z$  condition. The magnetic configuration of the source regions of the IMF associated with the ICME interval was also examined, which showed open magnetic field structures, emanating from a small active region on the north of the heliospheric current sheet (HCS). The structures remained constantly to the north of the HCS, both on 29 April and 1 May, suggesting no change in their polarity. The draping of these outward directed radial field lines around the propagating CMEs in the shocked plasma explains the observed polarity changes of the IMF- $B_z$  at 1 AU. In addition, multiple enhancements were also detected in the geomagnetic field variations, which showed a distinct one-to-one correspondence with the density pulses observed at 1 AU, during 0700–1700 UT on 3 May. The spectral analyses of both the variations showed the same discrete frequencies of 0.48, 0.65, and 0.75 mHz, demonstrating that the solar wind density enhancements can cause detectable global geomagnetic disturbances. The observations, thus, provide a deeper insight into the possible causes and geomagnetic consequences of a prolonged weakly southward IMF- $B_z$  condition.

### 1. Introduction

In spite of significant advances in both instrumental capabilities and theoretical simulations, our understanding of various aspects of solar wind-magnetosphere-ionosphere coupling is still far from comprehensive. Nevertheless, over the years, a consensus has been reached on the potential impact of the north-south component of the interplanetary magnetic field (IMF- $B_z$ ), which controls the amount of solar wind energy transferred into the magnetosphere through magnetic reconnection of the IMF- $B_z$  and the terrestrial magnetic field [e.g., *Dungey*, 1961]. The coupling is strongest when the IMF- $B_z$  is southward. The solar plasma moving with a velocity,  $V_{sw}$ , and having a frozen-in southward IMF- $B_z$  generates a dawn-to-dusk electric field,  $E_y = (-V_{sw} \times B_z)$  [*Tsurutani and Meng*, 1972; *Gonzalez et al.*, 1994; *Echer et al.*, 2008a]. The electric field is primary responsible for causing magnetic storms. It has been shown that it is the extraordinary and long duration southward IMF- $B_z$  events (magnitudes greater than  $-10$  nT and lasting for over 3 h), rather than high solar wind velocity, which plays a crucial role in triggering magnetic storms [*Gonzalez and Tsurutani*, 1987; *Tsurutani et al.*, 1992], and is therefore an important aspect for space weather studies.

The causes of strong and long duration southward IMF- $B_z$  events identified to date are either of solar or interplanetary origins. Events having solar origins are primarily associated with well-defined solar eruptive phenomena such as coronal mass ejection (CME) [*Klein and Burlaga*, 1982; *Lindsay et al.*, 1995], solar flares [*Tang et al.*, 1989], filament or prominence eruptions [*Tang et al.*, 1989], and high-speed solar wind streams from coronal holes (CHs) [*Sheeley et al.*, 1976]. The major southward IMF- $B_z$  events responsible for severe and

great storms are all caused by magnetic clouds within CMEs [Gosling *et al.*, 1990; Tsurutani *et al.*, 1992; Echer *et al.*, 2008b]. A CME is a huge eruption of coronal plasma and is classically composed of three parts [Illing and Hundhausen, 1986]. This includes (1) a leading edge, (2) a dark cavity, and (3) a bright core. The leading edge of the CME is mainly composed of coronal loops, and these have been detected at 1 AU [Tsurutani *et al.*, 1998], while the bright core is due to the cold and dense filament material [Webb and Hundhausen, 1987] which have also been detected at 1 AU. The filament is geoeffective [Kozyra *et al.*, 2014], while the loop is generally not [Tsurutani *et al.*, 2014]. The dark region of the CME is known as magnetic cloud [Burlaga *et al.*, 1981; Klein and Burlaga, 1982] and can be detected at 1 AU in in situ observations during the passage of the CME. They are usually characterized by a higher magnetic field strength than the ambient solar wind, a radial dimension of  $\sim 0.25$  AU at 1 AU, a smoothly rotating field direction, and low proton temperature [Tsurutani *et al.*, 1988]. More often all three components of a CME are not detected at 1 AU, and so in the interplanetary space a CME is known as interplanetary coronal mass ejection (ICME). ICMEs at 1 AU have been identified by observations of counterstreaming electrons with energies  $\geq 80$  MeV. This suggests that the ICME (with magnetic cloud (MC)) have a magnetic flux rope structure [Klein and Burlaga, 1982] with their ends anchored to the Sun. The radial fields rooted to the Sun are the “magnetic foot” regions of the ICME or the MC [Gosling *et al.*, 1974].

Events having interplanetary origins include those with shock compressed sheath fields [Tsurutani *et al.*, 1988; Echer *et al.*, 2008a], driver gas magnetic fields [Tang *et al.*, 1985; Tsurutani *et al.*, 1988; Tang *et al.*, 1989; Echer *et al.*, 2008a], draped interplanetary magnetic fields [Gosling and McComas, 1987; Tsurutani *et al.*, 1988; Echer *et al.*, 2008a], unusual or kinky heliospheric current sheets [Tsurutani *et al.*, 1984], and corotating interaction regions [Smith and Wolfe, 1976; Rosenberg and Coleman, 1980; Tsurutani *et al.*, 1995, 2006]. A small number of southward IMF- $B_z$  events are, however, caused by large-amplitude variations of intermittent Alfvénic turbulence, waves, or discontinuities [Tsurutani *et al.*, 1988, 1992]. In a study of the interplanetary causes of the extreme southward IMF- $B_z$  events responsible for major geomagnetic storms during 1978–1979, Tsurutani *et al.* [1988] reported that half of the southward IMF- $B_z$  events were caused by shock compressed sheath fields, while the other half were caused by driver gas fields or magnetic clouds (MCs). In a similar study during solar cycle 23, Echer *et al.* [2008a] also reported that intense southward IMF- $B_z$  events were caused by MCs which drove fast shocks causing 24% of the storms, sheath fields also causing 24% of the storms, and combined sheath and MC fields causing 16% of the storms. MCs are thus considered to be an important source of the southward IMF- $B_z$  events. In a recent study, Zhang and Moldwin [2014] reported a statistical study of solar sources of extreme, long duration, southward IMF- $B_z$  events (IMF- $B_z \geq 10$  nT and lasting for more than 6 h). A majority (53%) of these events were related to MCs, and 10% were related to ICME without MC signatures. For events associated with MC having shocks ahead, if there is already preexisting southward fields upstream of the shock, then the shock arrival compresses the fields and intensifies them [Tsurutani *et al.*, 1988, 2011]. Subsequently, as these southward fields approach the MC, the field lines drape around the MC plasma leading to strong southward fields [Gonzalez *et al.*, 1994], thereby resulting in a long duration southward IMF- $B_z$  event. It is to be noted though that the draping of the field lines around the CME depends on the CME trajectory, the direction of the radial interplanetary magnetic field (IMF), and the position of the heliospheric current sheet separating the positive and negative field lines [Gosling and McComas, 1987; McComas *et al.*, 1989].

Though many attempts have been made, it is not straightforward to determine the possible cause of prolonged southward IMF- $B_z$  events, and it is certainly more difficult when the southward IMF- $B_z$  is weak for prolonged intervals. The objective of the present paper is to investigate the cause of an extremely long duration ( $\sim 44$  h), weakly southward and relatively stable IMF- $B_z$  that gave rise to geomagnetic storm conditions during the period 2–4 May 1998. To the best of our knowledge, this is for the first time that such an unusually prolonged weakly southward IMF- $B_z$  and its possible solar or interplanetary causes are being reported. However, there are reports of extended periods of southward IMF- $B_z$  events, such as the weakly southward IMF- $B_z$  for  $\sim 12$  h on 13–14 February 2001 [Walker *et al.*, 2006] and for  $\sim 33$  h on 15–16 July 2012 [Bagiya *et al.*, 2014]. Tanskanen *et al.* [2005] also reported a long southward IMF- $B_z$  event of  $\sim 31$  h while studying magnetotail response of prolonged southward IMF- $B_z$  events lasting longer than 8 h during November 1999 through April 2002. However, none of these papers addressed their origin.

The geomagnetic response of such extreme and long duration southward IMF- $B_z$  events is generally a magnetic storm [Tsurutani and Meng, 1972; Gonzalez and Tsurutani, 1987; Tsurutani *et al.*, 1992] or a magnetic substorm [Tsurutani and Meng, 1972; Walker *et al.*, 2006]. However, during weakly southward IMF- $B_z$  fields, solar wind “ram” pressure changes ( $P_{\text{dyn}}$ ) become important. Variations in  $P_{\text{dyn}}$  commonly cause sudden impulses (SI) [e.g., Wilson and Sugiura, 1961; Russell *et al.*, 1994; Francia *et al.*, 2001; Villante *et al.*, 2005;

Villante and Piersanti, 2009] and are generally caused by arrival of interplanetary shocks at 1 AU [Sonett and Colburn, 1965]. On some occasions, pairs of sudden impulses or SI pairs, separated by a few hours, have been identified at ground stations [Rastogi et al., 2010]. Also, the interplanetary (IP) shocks (or ram pressure changes) could trigger substorms due to precursor southward IMF conditioning [Zhou and Tsurutani, 2001]. So, in general, it can be said that global geomagnetic disturbances caused by such abrupt changes in solar wind velocity have been of interest and have been studied in great detail over the years. Besides velocity the ram pressure changes depends on solar wind density, which plays a role in ring current intensification [Chen et al., 1994; Jordanova et al., 1998; Borovsky et al., 1998; Smith et al., 1999; Wang et al., 2003]. Even the ram pressure changes arising due to only high-density variations could externally trigger isolated intense substorm events or supersubstorms ( $AE \leq -2500$  nT) during storm or nonstorm conditions [Tsurutani et al., 2015]. However, studies on the impact of solar wind density variations on the geomagnetic environment are sparse.

The present prolonged southward IMF- $B_z$  event, on 2–4 May 1998, resulted in a mild storm on 2 May as well as an intense storm on 4 May [Ganushkina et al., 2005]. In addition to these storms, we also found quasiperiodic geomagnetic field variations for a duration from 0700 UT to 1700 UT on 3 May 1998. Corresponding to these quasiperiodic magnetic field variations, similar solar wind density variations were observed at 1 AU. So in the present investigation, based on a case study, we showed that solar wind density variations can affect geomagnetic field variations even during a long weakly southward and relatively stable IMF- $B_z$  condition.

It has also revealed by a spectral analysis of solar wind density variations having periodic or quasiperiodic fluctuations that they exhibit discrete frequencies [Kepko et al., 2002; Kepko and Spence, 2003; Viall et al., 2009a] or wavelengths [Viall et al., 2008]. These are particular frequencies or wavelengths, where the spectral analysis often shows significant power. Such frequencies have been found to occur at 0.7, 1.4, 2.0, and 2.7 mHz in the ultralow frequency (ULF) range. Kepko et al. [2002] and Kepko and Spence [2003] also reported such discrete frequencies in magnetospheric fields and concluded that the ULF fluctuations in solar wind density were the driver of magnetospheric field oscillations. Later, Kepko and Spence [2003] argued that the density fluctuations instead were actually periodic density structures (PDS) formed near the solar surface, which being frozen in the solar plasma, convect with the ambient solar wind to 1 AU. In a study of solar wind density fluctuations for 11 years during solar cycle 23, Viall et al. [2008] reported inherent radial scale sizes of PDS occurring at wavelengths of  $L \sim 73, 120, 136,$  and  $180$  Mm (for the slow wind) and  $L \sim 187, 270,$  and  $400$  Mm (for the fast wind). To find the sources of PDS, a series of papers, based on the study of alpha-to-proton solar wind abundance ratio [Viall et al., 2009b] and the remote observations of PDS using imaging data from *Solar Terrestrial Relations Observatory (STEREO)* spacecraft [Viall et al., 2010; Viall and Vourlidas, 2015], reported that they are formed in the variable coronal solar plasma around or below  $2.5 R_\odot$ , which advect with the slow solar wind to 1 AU. In the present paper, we also verified whether such discrete frequencies were present in both solar wind density and geomagnetic field variations during the period from 0700 UT to 1700 UT on 3 May 1998, when we found a clear one-to-one correspondence between the two.

### 1.1. Tracking of Solar Wind Events at 1 AU to Its Solar Source Region

Using in situ measurements, solar wind flows can be traced back, from the Earth's orbit (at 1 AU) to a solar source surface at  $2.5 R_\odot$ , where  $R_\odot$  is solar radius. Further, using measurements of photospheric magnetic fields and potential field computations, the flows can be mapped back to the Sun. Many examples exist of such studies, some of which are listed here. In order to study quadrupole distortions of the heliospheric current sheet, from May 1976 to May 1977, Bruno et al. [1982, 1984] successfully used the solar wind trace-back method in conjunction with a potential field model. In early 1995, using data obtained from the Ulysses and Wind spacecraft, Neugebauer et al. [1998] traced back solar wind structures to the source surface at  $2.5 R_\odot$  and then mapped them back to the photosphere. In an attempt to link outflows from an equatorial coronal hole and solar wind observed at 1 AU, McIntosh et al. [2011] used space-based data from the *Advanced Composition Explorer (ACE)* to trace the solar wind back to the source surface using potential field source surface models. To identify the source regions of gradual solar energetic particle (SEP) events at 1 AU, Ko et al. [2013] first used solar wind speed measurements to map the Sun-L1 interplanetary magnetic field lines back to its source regions on the Sun at the time of SEP observations and compared the characteristics of the SEP events to the identified sources of IMF.

**Table 1.** The Seven Indian Stations Are Listed in the Increasing Order of Their Magnetic Latitudes, Located Mainly at Low Latitudes<sup>a</sup>

Indian Stations	Magnetic Latitude (ML)
Trivandrum (TRD)	00.03°N
Pondicherry (PND)	03.07°N
Visakhapatnam (VSK)	08.56°N
Alibag (ABG)	10.36°N
Nagpur (NGP)	12.33°N
Shillong (SHL)	16.30°N
Gulmarg (GUL)	25.60°N

<sup>a</sup>The measurements from the stations were used to show the multiple geomagnetic field variations, during the period from 0700 to 1700 UT on 3 May 1998 as seen in Figure 4 (left).

The velocity traceback technique though is applicable only to steady state solar wind flows, however, it has also been successfully used even when the solar wind flows were highly nonradial [e.g. *Balasubramanian et al.*, 2003; *Janardhan et al.*, 2005, 2008a, 2008b] during the well-known solar wind disappearance event of 11 May 1999. To identify the solar source locations of the disappearance event, the authors traced back solar wind flows to the source surface at  $2.5 R_{\odot}$ , and using potential field computations [*Hakamada and Kojima*, 1999] mapped them back to the photosphere. From their study of the disappearance event of 11 May 1999, *Janardhan et al.* [2005] reported the maximum trace back errors to be  $\sim 30^{\circ}$ .

In this paper, we also used the two-step trace back method to locate the footpoints or the source region of the IMF associated with the prolonged IMF- $B_z$  event. In the first step, we traced back the field lines, using in situ measurements of solar wind speed from the ACE spacecraft at 1 AU, to the source surface at  $2.5 R_{\odot}$ . Following this, in the second step, using potential field computations [*Hakamada and Kojima*, 1999] to synoptic maps, we traced the field lines from the source surface back to the photosphere and investigated the background magnetic field conditions on the Sun during our period of interest.

It is important to note that generally in such potential field models, the coronal magnetic field below the source surface is assumed to be quasi-stationary, while it is considered to be open beyond the source surface. Also, it is to be noted that the tracing of the source region and magnetic field lines, using a Carrington synoptic

magnetogram, has to be carefully treated at the two ends of a magnetogram. The magnetic field at this region changes faster than the normal level, which can lead to variations in the tracing process and the extrapolations of the magnetic field lines [*Huang et al.*, 2014]. However, for our 2–4 May 1998 event, the Carrington longitude was close to the center of the magnetogram, so the boundary effect would not be significant.

**Table 2.** The Seventeen Stations of 210 MM Network and Their Magnetic Latitudes Are Shown<sup>a</sup>

210 MM Stations	Magnetic Latitude (ML)
Kotel'nyy (KTN)	69.64°N
Tixie (TIK)	65.67°N
Chokurdakh (CHD)	64.67°N
Zyryanka (ZYK)	59.62°N
Magadan (MGD)	53.56°N
Moshiri (MSR)	37.61°N
Popov Island (PPI)	36.62°N
Onagawa (ONW)	24.85°N
Kagoshima (KAG)	25.13°N
Yamakawa (YMK)	13.80°N
Lunping (LNP)	10.36°N
Guam (GAM)	04.57°N
Muntinlupa (MUT)	03.58°N
Biak (BIK)	12.18°S
Learmonth (LMT)	34.15°S
Canberra (CAN)	45.98°S
Katanning (KAT)	46.03°S

<sup>a</sup>The stations are located at latitudes starting from low through mid and on to high latitudes. Thirteen of them are in the Northern Hemisphere, while four of them are in the Southern Hemisphere. The measurements from the stations were used to show the multiple geomagnetic field variations, during the period from 0700 to 1700 UT on 3 May 1998, as seen in Figure 4 (right).

## 2. Presentation of Data

For IMF and solar wind observations at 1 AU, we have used data available in the public domain from <http://cdaweb.gsfc.nasa.gov/cgi-bin/eval2.cgi>. For interplanetary plasma and IMF data such as solar wind proton velocity and the strength of IMF we have used data obtained from the ACE spacecraft [*Stone et al.*, 1998]. Ground-based measurements of solar wind velocities in the inner heliosphere, using radio observations of interplanetary scintillation at 327 MHz [*Kojima and Kakinuma*, 1990], were also utilized. For studying the photospheric magnetic field distribution, synoptic magnetograms, made using data from the *Michelson-Doppler-Interferometer (MDI)* [*Scherrer et al.*, 1995] instrument on

board the *Solar and Heliospheric Observatory (SOHO)* [Domingo *et al.*, 1995], were used. Measurements of ground magnetic deviations were obtained from both Indian stations and the 210° magnetic meridian (210 MM) network [Yumoto and CPMN Group, 2001]. The seven Indian and seventeen 210 MM stations used have been shown in Tables 1 and 2. The Indian stations are mainly located at low latitudes, while the 210 MM network of stations is located at latitudes starting from low through mid and on to high latitudes. Of these 17 stations, 13 are located in the Northern Hemisphere, while 4 are in the Southern Hemisphere.

### 2.1. Interplanetary Scintillation Observations

Interplanetary Scintillation (IPS), typically observed at meter wavelengths, is a diffraction phenomenon in which coherent electromagnetic radiation from a distant radio source passes through the turbulent, refracting solar wind and suffers scattering, thereby resulting in random temporal variations of the signal intensity (scintillation) at the Earth. A schematic illustration of the typical IPS observing geometry can be seen in Biso *et al.* [2014a]. IPS is an efficient, cost-effective method of studying the large-scale structure of the solar wind at meter wavelengths, over a wide range of heliocentric distances, ranging from about 0.2 AU to 0.8 AU at 327 MHz [Hewish *et al.*, 1964; Janardhan and Alurkar, 1993; Ananthakrishnan *et al.*, 1995; Janardhan *et al.*, 1996; Moran *et al.*, 2000; Biso *et al.*, 2014a]. Intensity variations from point-like extragalactic radio sources, during IPS observations, actually provide remote sensing information about RMS electron density fluctuations,  $\Delta N_{\text{RMS}}$ , along the lines of sight to the observed radio sources [Biso *et al.*, 2014a]. In fact, IPS is so sensitive to changes in  $\Delta N_{\text{RMS}}$  that it has even been used to study the fine-scale structure in cometary ion tails during radio source occultations by cometary tail plasma [Janardhan *et al.*, 1991, 1992; lju *et al.*, 2015]. IPS data were obtained from the Institute for Space-Earth Environmental Research (ISEE), Nagoya University, Nagoya, Japan, and using a tomographic technique, IPS observations from ISEE, Japan were used to produce synoptic velocity maps [Kojima *et al.*, 1998] which were then projected back to a fixed heliocentric distance, *viz.* the source surface, at  $2.5 R_{\odot}$ . Such synoptic velocity maps represent the large-scale structure of the solar wind in the inner heliosphere.

## 3. A Prolonged Southward IMF- $B_z$ Event

Figure 1 presents solar wind conditions at 1 AU (measurements of solar wind magnetic field and plasma) of an event on day of 1.5–4.5 in May 1998 and the state of magnetospheric response associated with the event. Figure 1 (first panel) shows the southward component of interplanetary magnetic field ( $B_z$ ). An unusually prolonged southward IMF- $B_z$  lasting for a period of  $\sim 44$  h, from 0920 UT on 2 May to 0520 UT on 4 May, is clearly evident as shown by the solid red line in Figure 1 (first panel). To identify the cause of such a prolonged southward IMF- $B_z$  condition, we first studied the interplanetary (IP) disturbances associated with the event through solar wind parameters such as magnitude of magnetic field ( $B$ ), proton velocity ( $V_p$ ), proton density ( $N_p$ ), and proton temperature ( $T_p$ ) as shown in Figure 1 (second to fifth panels), respectively.

A forward shock was identified at 2123 UT on 1 May as indicated by a vertical dash-dotted line (S1). The arrival of the shock increased the proton density ( $\sim 20 \text{ cm}^{-3}$ ), velocity ( $600 \text{ km}^{-1}$ ), and temperature ( $\sim 10^{10} \text{ K}$ ), as well as the magnetic field intensity ( $\sim 20 \text{ nT}$ ). Prior to the shock, the magnitude of IMF was high ( $\sim 10 \text{ nT}$ ), and the IMF- $B_z$  was  $\sim 0 \text{ nT}$  6 h before and  $\sim +7 \text{ nT}$  just 30 min before. The solar wind plasma preconditions were as follows:  $B$  was  $\sim 10 \text{ nT}$ ,  $V_p$  was  $\sim 300 \text{ km}^{-1}$ , and  $N_p$  was  $\sim 10 \text{ cm}^{-3}$ . Postshock, the IMF- $B_z$  showed rapid fluctuations, and the average IMF- $B_z$  was northward having  $\sim +10 \text{ nT}$ . However, the field actually turned first southward ( $B_z$  was  $\sim -8 \text{ nT}$ ) from the northward direction ( $B_z$  was  $\sim 10 \text{ nT}$ ) at 0300 UT on 2 May upon arrival of an ICME at 1 AU, marked by a vertical solid line (C). The arrival of ICME at 1 AU has been characterized by jumps in  $V_p$ ,  $N_p$ , and  $T_p$ , and a decrease in  $B$ . However, until 0920 UT, the southward field was not stable and showed a second southward turning only at 0920 UT on 2 May. Thereafter, the IMF- $B_z$  was constantly southward and relatively stable for the next 24 h.

The solar wind plasma during the prolonged period of weakly southward IMF- $B_z$  condition showed constant high-magnetic field intensity than the ambient field and continuous low proton temperature. These are typical signatures of the presence of a driver gas plasma or magnetic cloud (MC). The passage of the MC [Malandraki *et al.*, 2002] is indicated by vertical dashed lines in Figure 2. Malandraki *et al.* [2002] reported two prompt electron events as detected by ACE spacecraft during the passage of ICME, one when the CME leading edge arrives at 1 AU and the other when the front of MC passes at 1 AU. The monotonic decreases in both magnetic field and proton speed suggest that the ICME was expanding. Since the MC was traveling for

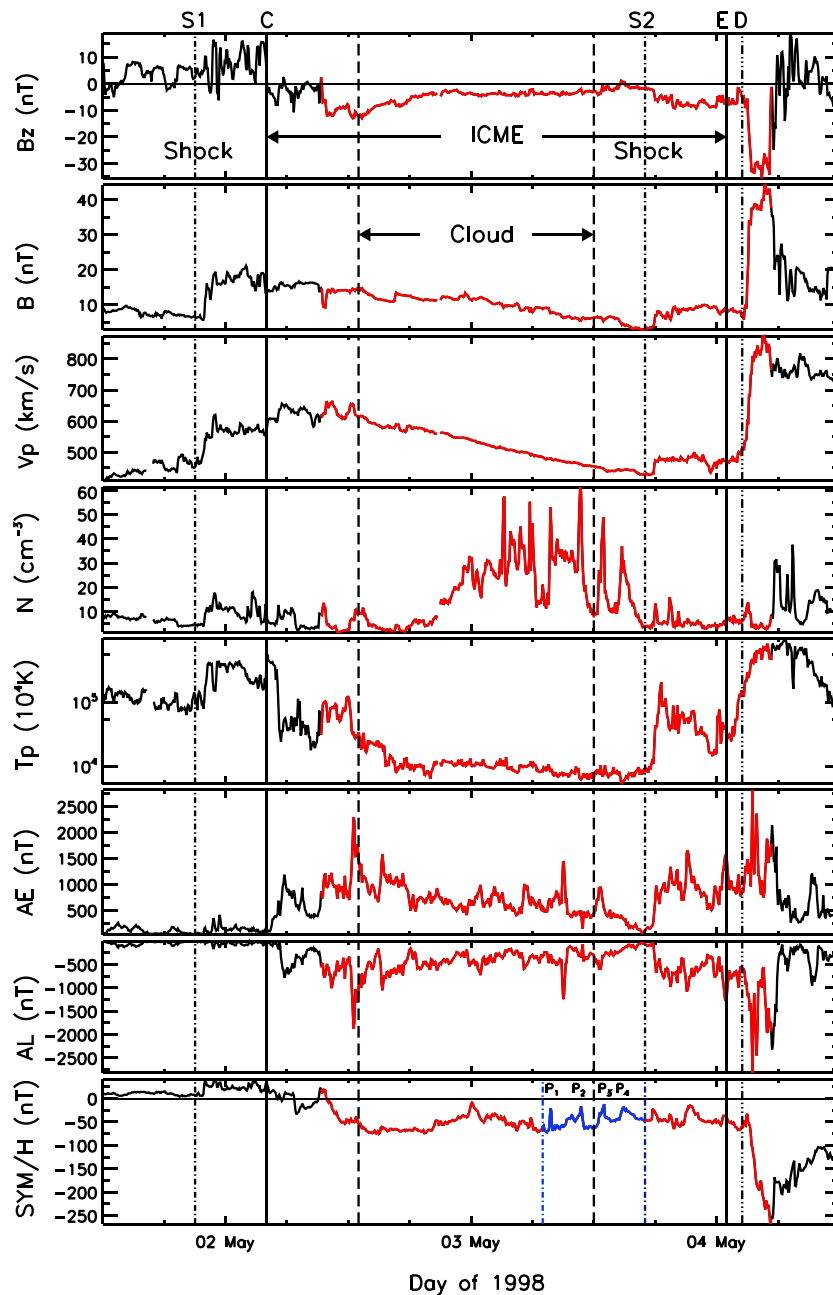


**Figure 1.** Spacecraft measurements of (first panel) IMF- $B_z$ , (second panel) magnitude of magnetic field, (third panel) proton velocity, (fourth panel) density and (fifth panel) temperature, and ground measurements of (sixth panel) AE, (seventh panel) AL, and (eighth panel) SYM-H indices on day of 1.5–4.5 in May 1998. The two vertical dash-dotted lines (S1 and S2) and the vertical long dash-dotted line (D), respectively, mark the arrival of shocks and discontinuity, while the two solid lines (C and E) mark the arrival and end of CME, respectively. The vertical dashed lines indicate the start and end of magnetic cloud. An unusually prolonged southward IMF- $B_z$  for a period of ~44 h is shown by the red solid line. The multiple enhancements observed in SYM-H index, during 0700 UT–1700 UT on 3 May, have been shown by the blue solid line, indicated between the blue vertical dash-dotted lines.

around 24 h with an approximate speed of  $500 \text{ km}^{-1}$ , it suggests that the radial dimension of the MC was  $\sim 0.28 \text{ AU}$ , which is the typical radial width of a MC as mentioned earlier. Also, a high-density plasma parcel ( $30\text{--}60 \text{ cm}^{-3}$ ) was located between 1800 UT on 2 May and 1700 UT on 3 May, for about 24 h. The density parcel, in fact, showed periodic/quasiperiodic density variations. The  $\text{He}^{++}/\text{H}^+$  ratio (though not shown here) had also shown significantly increased values, as high as 80% [Skoug et al., 1999].

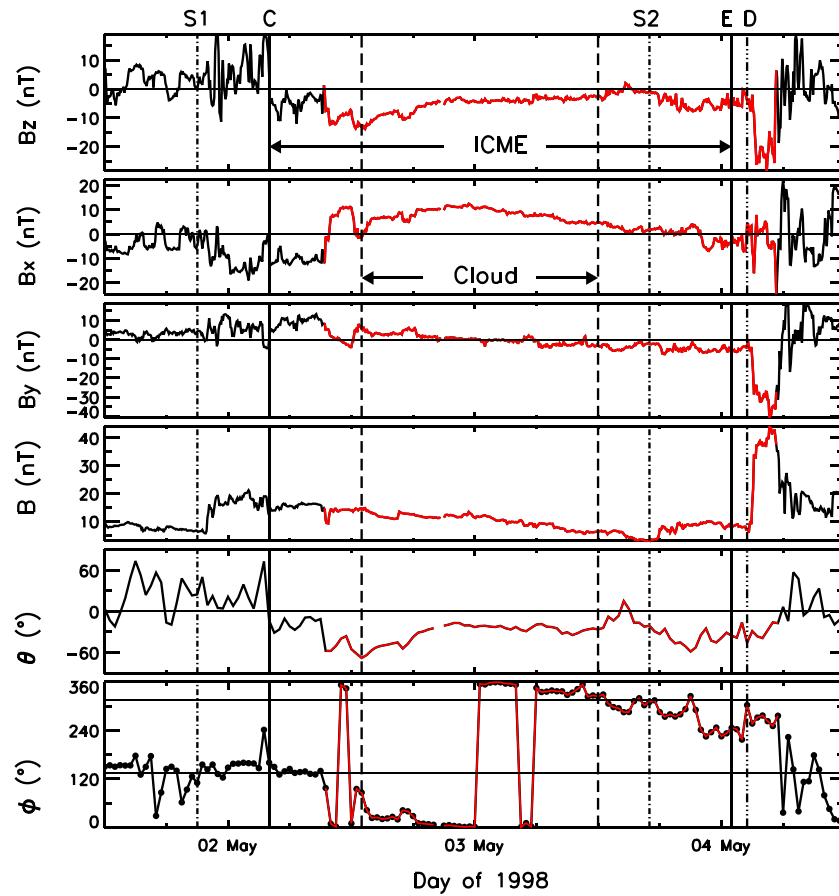


**Figure 2.** In situ measurements of magnitude and direction of the magnetic field (first to sixth panels)  $B_z$ ,  $B_x$ ,  $B_y$ ,  $B$ ,  $\theta$ , and  $\phi$ , respectively, on day of 1.5–4.5 in May 1998. The two vertical dash-dotted lines (S1 and S2) and the vertical long dash-dotted line (D), respectively, mark the arrival of shocks and discontinuity. The two solid lines (C and E) mark the arrival and end of CME, respectively, while the vertical dashed lines indicate the start and end of magnetic cloud. The steady state configuration of the IMF with  $\phi = 135^\circ$  or  $315^\circ$  is shown by the solid lines in Figure 2 sixth panel.

A second forward shock was identified at 1700 UT on 3 May, indicated by a vertical dash-dotted line (S2). The arrival of shock showed a small jumps in  $V_p$ ,  $N_p$ ,  $T_p$ , and  $B$  compressing the already preexisting southward fields and intensifying them further. Prior to the shock, the solar wind plasma preconditions were as follows:  $B$  was  $\sim 0$  nT,  $V_p$  was  $\sim 300$   $\text{kms}^{-1}$ , and  $N_p$  was  $\sim 8$ – $10$   $\text{cm}^{-3}$ . The IMF- $B_z$  was  $\sim 0$  nT just 2 h before. The shock was propagating back of the first ICME and was associated with a second ICME arriving later [Malandraki et al., 2002]. The end of ICME interval (E), shown by a vertical solid line, was observed with a decrease in  $T_p$ . Just prior to the end of ICME, when the southward field was slowly turning northward, a strong interplanetary discontinuity was identified, indicated by a vertical long dash-dotted line (D). Postdiscontinuity, the solar wind showed high jumps in  $V_p$ ,  $N_p$ ,  $T_p$ , and  $B$ ; however, these variations occurred over an extended period suggesting that it was not a shock. The discontinuity compressed the weak preexisting southward fields and intensifying them further ( $B_z$  decreases from  $-5$  nT to  $-32$  nT). The variations in solar wind plasma composition and properties during 2–4 May 1998 have been very well studied and reported by other researchers [e.g., Gloeckler et al., 1999; Skoug et al., 1999; Chen and Fritz, 1999, 2001; Bamert et al., 2002; Malandraki et al., 2002; Posch et al., 2003; Ganushkina et al., 2005].

### 3.1. Orientation of the Magnetic Fields

Figure 2 shows, from first to sixth panels, the magnetic field components ( $B_z$ ,  $B_x$ ,  $B_y$ ) in Geocentric Solar Ecliptic (GSE) coordinates, the magnitude of magnetic field ( $B$ ), and the direction of magnetic field ( $\theta$  and  $\phi$ ). In the GSE coordinate system, the  $X$  axis points from the Earth to the Sun, the  $Z$  axis is normal to the ecliptic, and the  $Y$  axis forms a right-hand coordinate system. The angle  $\theta$  is the angle of the magnetic field out of the ecliptic plane, while the angle  $\phi$  is the angle that the magnetic field makes with the  $X$  axis in the  $XY$  plane.

Before the passage of the MC, the magnetic field showed rapid fluctuations, while it was very smooth during its passage, as indicated by the low variance in the magnitude of magnetic field. From Figure 2, it is clear that the  $B_x$  component remained positive during MC traversal, while the  $B_z$  component was negative. However, the  $B_y$  component showed a change from positive to negative, indicating the usual directional changes noticed during the MC traversal. The typical Parker's spiral configuration of the IMF has values of  $\phi = 135^\circ$  or  $315^\circ$ , which corresponds to the positive or the negative IMF, respectively, shown by the horizontal lines in Figure 2 (sixth panel). The value  $\theta = 90^\circ$  usually denotes the position of the ecliptic North Pole. It is seen from Figure 2 that  $\theta$  was negative during the whole event. The IMF turned southward (negative  $\theta$ ), upon the arrival of the ICME, and continued to be thereafter southward until 4 May. The angle  $\phi$  was around  $135^\circ$  from 00 UT to 08 UT on 2 May, indicating a steady state configuration with a positive IMF. The first crossing of the IMF was noticed just prior to the MC, and on its arrival, the IMF became nonsteady for a while. The second crossing of the IMF was seen early on 3 May, from positive to negative, corresponding to the directional changes in the  $B_y$  component. Thereafter, the angle  $\phi$  was continued to be around  $315^\circ$  until 1700 UT on 3 May, indicating a steady negative IMF configuration, which again became nonsteady upon the arrival of the shocks driven by the second ICME from 1700 UT on 3 May to early on 4 May.

### 3.2. Geomagnetic Consequences

The magnetospheric response corresponding to the unusually prolonged southward IMF- $B_z$  condition on 2–4 May has been shown in Figure 1 (sixth to eighth panels), which show ground measurements of the auroral electrojet index ( $AE$ ), the westward electrojet index ( $AL$ ), and the symmetric ring current index ( $SYM-H$ ). On arrival of the first forward shock, S1, a sudden increase in  $SYM-H$  index ( $\geq 25$  nT), i.e., a positive sudden impulse (SI), was observed. However, only a very small increase in  $AE$  and  $AL$  indices was noticed. The arrival of the ICME, that caused the first southward turning of the IMF- $B_z$  field and the reverse shock, initiated a depression in  $SYM-H$  index early on 2 May at 0400 UT. So the arrival of forward and reverse shocks caused, respectively, a positive and a negative SI, as shown in the study by *Rastogi et al.* [2010]. The  $AE$  and  $AL$  indices, respectively, showed increases up to  $\sim 1000$  nT and  $\sim -800$  nT indicating onset of a moderate substorm activity. A moderate storm ( $SYM-H \leq -80$  nT) actually began on the second southward turning of the IMF- $B_z$  when the southward IMF- $B_z$  field intensified ( $B_z \leq -10$  nT) further. Correspondingly,  $AE$  and  $AL$  indices showed much higher values, indicating the progression of a substorm activity. At about 1300 UT on 2 May, their amplitudes had values greater than  $-1500$  nT, indicating an intense substorm activity in progress. Besides, the southward preconditioning, the solar wind plasma density was found to be higher ( $\sim 10$ – $15$   $\text{cm}^{-3}$ ), coincident with the substorm event. The increased solar wind density could have externally triggered the intense substorm activity.

Thereafter, on weakening of the southward field, the storm entered into the recovery phase as indicated by the slow increase in  $SYM-H$  index. The passage of a high-density plasma parcel early on 2 May further caused a depression in  $SYM-H$  index. In fact, multiple enhancements in  $SYM-H$  index were identified, shown by the blue solid line and demarcated by the vertical blue dash-dotted lines in Figure 1 (eighth panel), from 0700 UT–1700 UT on 3 May, during the steady weakly southward IMF- $B_z$  condition. The multiple peaks in  $SYM-H$  occurred at 0725 UT, 1010 UT, 1210 UT, and 1430 UT and were referred to in the rest of the paper as  $P_1$ ,  $P_2$ ,  $P_3$ , and  $P_4$ , respectively. During this steady weakly southward IMF- $B_z$  condition, we found fairly frequent changes in both  $AE$  and  $AL$  indices indicating a fair substorm activity. The arrival of the second forward shock again caused sharp increases in  $AE$  and  $AL$  indices that led to the onset of a moderate substorm activity. Subsequently, the arrival of the IP discontinuity caused a strong intensification of the southward IMF fields and resulted in an intense geomagnetic storm that began early on 4 May. Correspondingly, the  $SYM-H$  index showed a strong positive SI followed by a strong depression in its strength ( $\leq -250$  nT). Also, we found substantial enhancements in  $AE$  index ( $\geq 2500$  nT) as well as in  $AL$  index ( $\leq -2500$  nT) that led to a large substorm expansion.

It is thus clear that during the prolonged southward IMF- $B_z$  condition of 2–4 May, a constant geomagnetic activity with values of  $SYM-H \leq -50$  nT and a fairly constant substorm activity with values of  $AE \geq 500$  nT were observed prior to the onset of the great storm on 4 May. The storms during 2–4 May have been very well studied [*Chen and Fritz*, 1999, 2001; *Bamert et al.*, 2002; *Posch et al.*, 2003; *Ganushkina et al.*, 2005]. However, the multiple enhancements noticed in  $SYM-H$ , during the prolonged quasi-stable southward IMF- $B_z$  condition on 3 May, are unique and are being reported for the first time. We discuss them in detail in the following section.

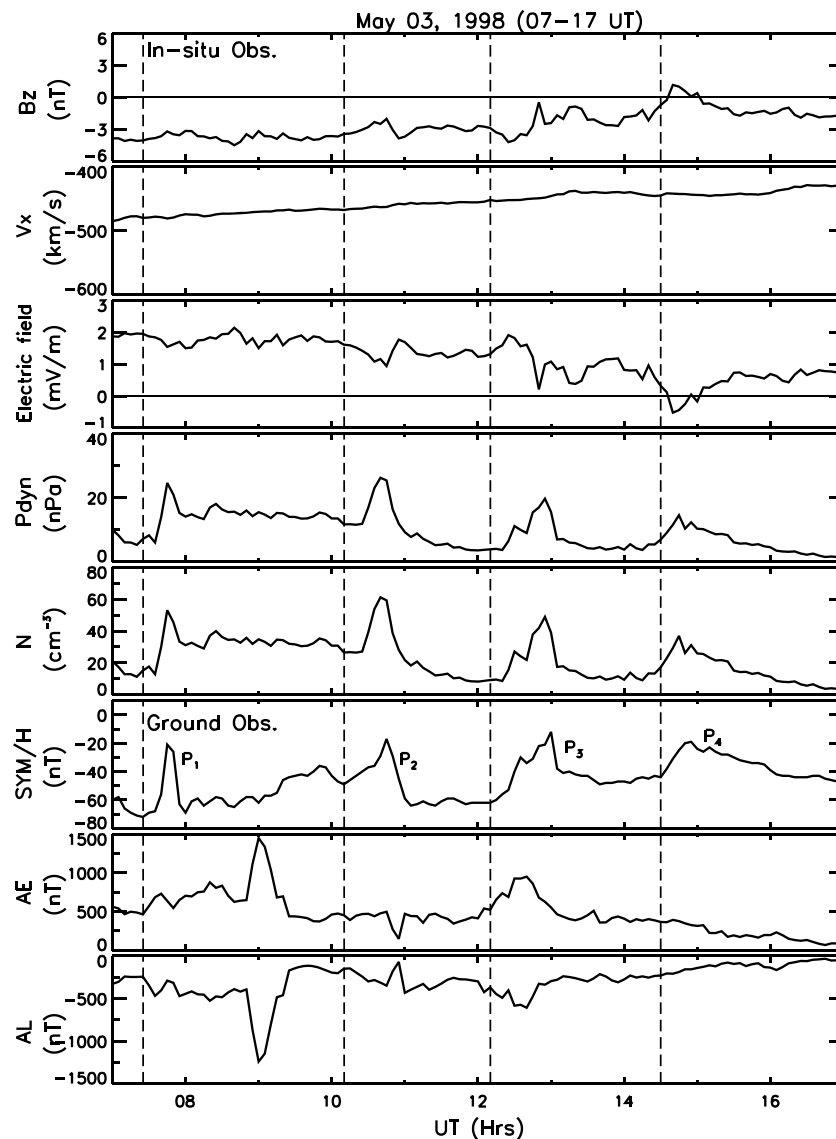


**Figure 3.** (first to eighth panels) Variations of the  $B_z$ , solar wind velocity, electric field, flow pressure, solar wind density,  $SYM-H$ ,  $AE$ , and  $AL$  as a function of time in UT on 3 May 1998, respectively. The vertical dashed lines demarcate the occurrence of multiple enhancements in  $SYM-H$  when there are no corresponding significant variations in both the IMF- $B_z$  and solar wind velocity. The multiple peaks in  $SYM-H$  are numbered from  $P_1$  through  $P_4$ , and corresponding to these pulses, multiple enhancements in solar wind dynamic pressure and solar wind density have also been identified.

#### 4. Multiple Pulses in the Geomagnetic Field Variations

As mentioned earlier, as a geomagnetic response to the quasi-stable southward IMF- $B_z$  condition during 3 May 1998, we identified the occurrence of multiple enhancements in the Earth's magnetic field as seen by the multiple pulses in  $SYM-H$  index during 0700 UT–1700 UT on 3 May. Starting from the top and going down, Figure 3 (first to eighth panels) shows, respectively, the IMF- $B_z$ , the component of solar wind velocity in the  $X$  direction ( $V_x$ ), the  $Y$  component of the interplanetary electric field ( $IEF_y$ ), the solar wind dynamic pressure ( $P_{dyn}$ ), the solar wind proton density ( $N$ ), the  $SYM-H$  index, the  $AE$  index, and the  $AL$  index for the period 0700 UT–1700 UT on 3 May. The multiple pulses are numbered from  $P_1$  through  $P_4$  and have also been shown in Figure 1 (eighth panel).

Corresponding to the multiple peaks in  $SYM-H$ , we identified multiple enhancements in solar wind dynamic pressure and solar wind density, indicated by the dashed vertical lines in Figure 3. These density variations are specifically of interest, as there were no significant variations observed in the IMF- $B_z$ , solar wind velocity,

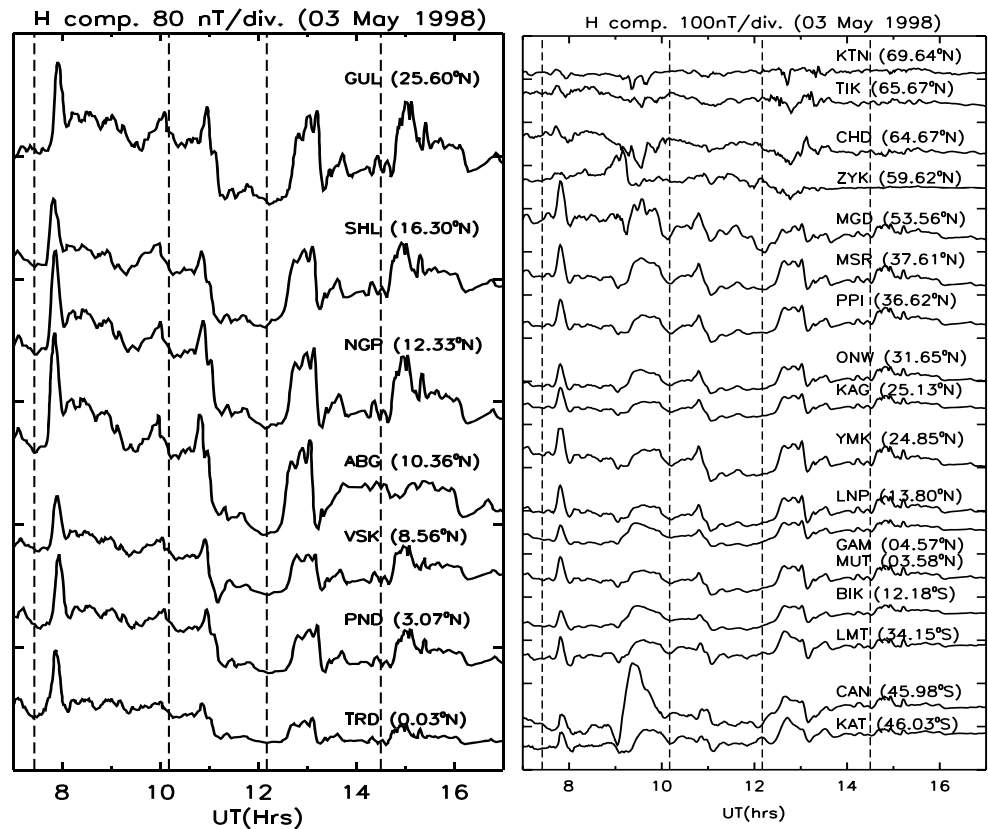


**Figure 4.** Variations of the horizontal component (H-comp) of the Earth's magnetic field for (left) Indian stations and (right) 210 MM stations between 0700 UT and 1700 UT on 3 May 1998. Shown on the right of each curve is the geomagnetic latitude of each station. The vertical dashed lines have been marked at the time of onset of pulses  $P_1$ ,  $P_2$ ,  $P_3$ , and  $P_4$ , respectively, in the  $SYM-H$  field.

and the  $IEF_y$  except for the corresponding deviations in the  $SYM-H$ . We also did not see much variation in both  $AE$  and  $AL$  indices corresponding to the peaks in the  $SYM-H$  field. It is important to note that the surface magnetic deviations in the  $SYM-H$  have a distinct one-to-one correspondence both in time and profile with that of the solar wind density pulses. Since the  $SYM-H$  field represents the mean variation of the  $H$  field at all midlatitude ground stations, the observed deviations showed that the event is a global one. Further, we have taken care to verify that the  $SYM-H$  pulses were global by examining records of the change in the horizontal component of geomagnetic field ( $\Delta H$ ) from ground-based magnetograms obtained from Indian magnetic observatories as well as from the 210 MM magnetic stations.

#### 4.1. Geomagnetic Field Variations at Indian and 210 MM Stations

Figure 4 shows the  $H$  variations, from 0700 to 1700 UT on 3 May 1998, for seven Indian stations (left) and seventeen stations of 210 MM network (right) with the magnetic latitude (ML) of each ground station indicated at the right of each curve. The magnetic latitudes of Indian and 210 MM network stations shown in Figure 4 have already been listed in Tables 1 and 2. It is evident from Figure 4 that the  $H$  variations from 0700 to 1700 UT for both the Indian (Figure 4, left) as well as the 210 MM stations (Figure 4, right), had shown increases corresponding to the pulses  $P_1$ ,  $P_2$ ,  $P_3$ , and  $P_4$ . Only for the case of pulse  $P_3$ , as already noticed from the variation of the  $AE$  and  $AL$  indices shown in Figure 3, we found signatures of positive and negative bays [e.g., Russell et al., 1994] on inspection of the  $H$  variations of 210 MM stations. The  $H$  variations at the Indian and the 210 MM stations are synchronous at all latitudes and have been marked by the vertical dashed lines in Figure 4 (left and right). It is to be noted that these deviations in the  $H$  field, as stated earlier, have clearly shown a one-to-one correspondence with the episodic enhancements in the solar wind density as shown in Figure 3.

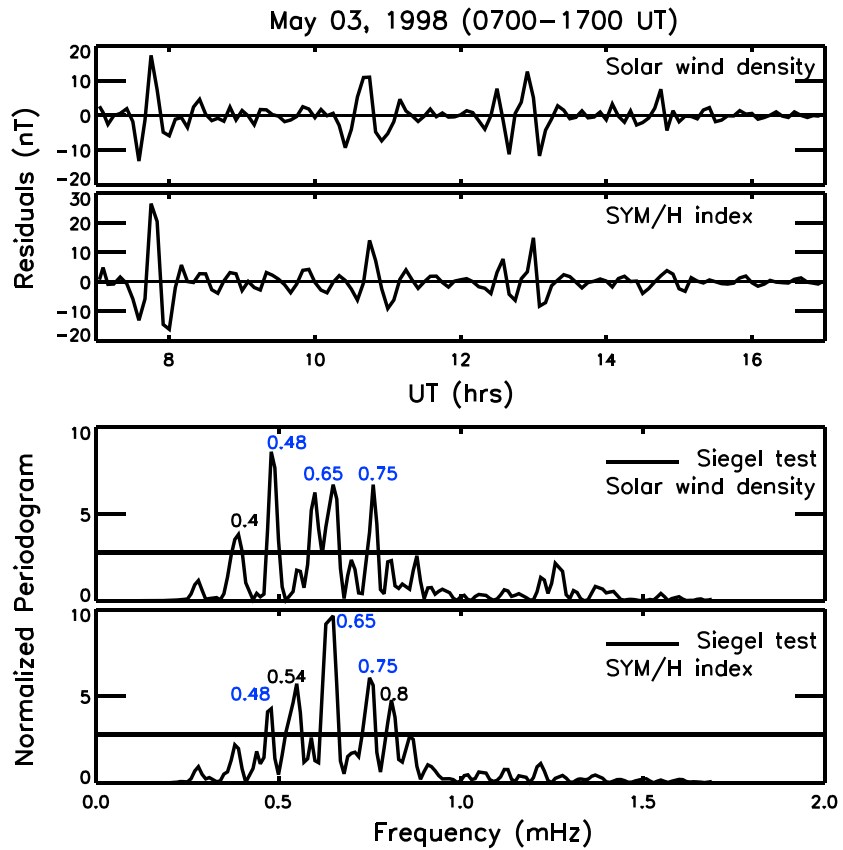


**Figure 5.** (top two panels) Variation of the residuals of solar wind density and *SYM-H* field during the period from 0700 to 1700 UT on 3 May. (bottom two panels) The Lomb-Scargle normalized periodograms. The black horizontal lines shown in Figure 5 (bottom two panels) are drawn at critical level determined by the Siegel test statistics.

#### 4.2. Discrete Frequencies of Density and Geomagnetic Field Fluctuations

It is evident from Figure 3 that, during the period from 0700 to 1700 UT on 3 May 1998, the solar wind density changes and geomagnetic field variations were quite similar. The same also can be clearly seen from their residuals, as shown in Figure 5 (top two panels). Though the existence of quasiperiodic variations is clear from the residuals of density and *SYM-H* index, however, it is difficult to pinpoint the discrete frequencies at which they occurred. We, thus, subjected the residuals of solar wind density and geomagnetic field variations to a Lomb-Scargle Fourier transform [Lomb, 1976; Scargle, 1982, 1989] to find the discrete peaks.

Figure 5 (bottom two panels) shows the Lomb-Scargle normalized periodograms of solar wind density and *SYM-H* field obtained for the period from 0700 to 1700 UT on 3 May. The significant frequency components were determined using the Siegel test statistics [Siegel, 1980; Bisoi et al., 2014b]. The black horizontal lines in Figure 5 (bottom two panels) are drawn at the critical level determined by the Siegel test. From Figure 5, it is clear that the density and geomagnetic field pulsations have peaks near frequencies,  $f = 0.48, 0.65,$  and  $0.75$  mHz, or periods,  $T = 35, 26,$  and  $22$  min. The frequency peaks reported here belong to the long period or ULF oscillations. In addition, to the common frequencies, the density data also exhibit a peak near  $f = 0.4$  mHz, while the *SYM-H* field show peaks near  $f = 0.54$  and  $0.8$  mHz. As discussed earlier, the periodic density variations are actually PDS that are present in the solar wind. The PDS are formed near the solar surface and convect with the ambient solar wind to 1 AU. Based on this fact, we computed the length scales of the PDS, using the method followed by Kepko and Spence [2003] and Viall et al. [2008], defined as the wavelength,  $L = \langle V_x/f \rangle$ , where  $V_x$  is the solar wind velocity and  $f$  is the observed discrete frequency. The radial scale sizes of the density structures were thus found to occur at  $L = 600, 704, 756, 947,$  and  $1160$  Mm.

## 5. Solar Sources of the Event

### 5.1. Flare and CME Observations

From the end of April to the beginning of May 1998, several flares/CMEs erupted on the Sun [Thompson *et al.*, 2000]. A “halo” CME was captured by the Extreme Ultraviolet Imaging Telescope (EIT) on board SOHO on 29 April at 1600 UT and by the *Large Angle and Spectrometric Coronagraph* (LASCO) [Brueckner *et al.*, 1995] instrument on board SOHO on 29 April at 1658 UT [Bamert *et al.*, 2002; Malandraki *et al.*, 2002]. Just prior to the eruption of the CME, an M-class flare (M6.8) erupted at 1606 UT on 29 April. It has been reported that though the flare and filament eruption occurred in the southeast (S17E16) of the disk center from an active region AR 8210, the CME moved across the equator and appeared in the northeast limb [Wang *et al.*, 2000]. The shock driven by the CME on 29 April reached at 1 AU at 2123 UT on 1 May, while the leading edge of the CME arrived at 0300 UT on 2 May [Malandraki *et al.*, 2002]. An X class flare and another fast halo CME were detected in SOHO/EIT at 1340 UT and in LASCO/C2 at 1406 UT on 2 May, respectively. The flare and CME were produced in the southwest (S15W15) from AR 8210 [Thompson *et al.*, 2000]; however, the CME moved across the equator and appeared in the northwest limb as seen from LASCO/C2 images [Wang *et al.*, 2002]. The shock driven by the second CME traveled behind the first CME and arrived at 1 AU at 1700 UT on 3 May.

## 6. In Situ Magnetic Field and Remote-Sensed IPS Observations

A study of the observation of bidirectional electron events from the Electron, Proton, Alpha Monitor on board ACE (ACE/EPAM) [Malandraki *et al.*, 2002] has reported that the magnetic field lines at 1 AU during the ICME traversal were magnetically anchored to the Sun. To verify the background IMF conditions associated with the event, we traced back in situ measurements of solar wind speed (and the associated IMF) from the ACE spacecraft at 1 AU to the source surface at  $2.5 R_{\odot}$ , assuming constant velocities and radial expansion along the Parker’s spirals. The arrival of CMEs, in the present case, could have actually caused deviations in the Parker’s spiral resulting in the highly nonradial flows [Owens and Cargill, 2004]. However, we could still use the trace back method considering the fact that the source regions of flows (and the IMF) determined would be within reasonable errors. We verified (though not shown here) from the deviations of the solar wind flow velocities estimated using in situ measurements of ACE spacecraft that the flows during 2–4 May were largely radial. They only became highly nonradial right after the arrival of the second CME on 4 May. Also, the value of  $\phi$  remained around  $135^{\circ}$  or  $315^{\circ}$ , as shown in Figure 2 (sixth panel), indicating a steady state IMF configuration.

The heliographic latitude and longitude of the source regions of the IMF at  $2.5 R_{\odot}$  were first obtained by transforming the available positions of ACE spacecraft at a particular time from the GSE coordinates to Carrington coordinates. The heliographic latitude at the source surface is generally same as that of the heliographic latitude of the ACE spacecraft. However, the heliographic longitude at the source surface was obtained by adding an offset to the heliographic longitude of ACE at 1 AU [Huang *et al.*, 2014]. The offset was determined by estimating the longitude through which the Sun had rotated during the solar wind propagation time from the source surface to 1 AU using the velocity trace back method.

The topmost panel of Figure 6 shows ACE measurements of proton velocities traced back to the source surface at  $2.5 R_{\odot}$  as a function of heliographic longitude. The red dashed vertical lines, marked at the heliographic longitudes of  $128^{\circ}$  and  $158^{\circ}$ , indicates the day of year (DOY) 119.72–121.98 (1716 UT, 29 April to 1 May, 2331 UT) corresponding to the trace back locations of the solar wind velocities (or the associated IMF) at 1 AU, during our period of interest from the DOY 122.39–124.22 (0920 UT, May 02–0520 UT, May 04).

The heliographic latitude of the traced back velocities/IMF at the start and the end of the period of interest was found to be  $\sim -4^{\circ}$  and  $\sim -5^{\circ}$ , respectively. The blue vertical solid line indicates the trace back locations of the IMF corresponding to the onset of a SI prior to a strong geomagnetic storm on 4 May. Dates of Central Meridian Passage (CMP) are indicated at the top of Figure 6 (top). From Figure 6 (top), it is clear that during this period the proton velocity showed a steady increase from  $400 \text{ km s}^{-1}$  to  $820 \text{ km s}^{-1}$  without much fluctuations, indicating the increase in velocity could be due to the eruption of CME on April 29.

Figure 6 (middle) shows a tomographic synoptic velocity map for CR1935. The velocity map was obtained using IPS observations from the ISEE, Japan, and represents solar wind velocities projected on to the source surface at  $2.5 R_{\odot}$ . The white regions on the map indicate data gaps, while the color bar on the right shows the velocity of solar wind flow. The curved black line on the map is the source surface magnetic neutral line (MNL).

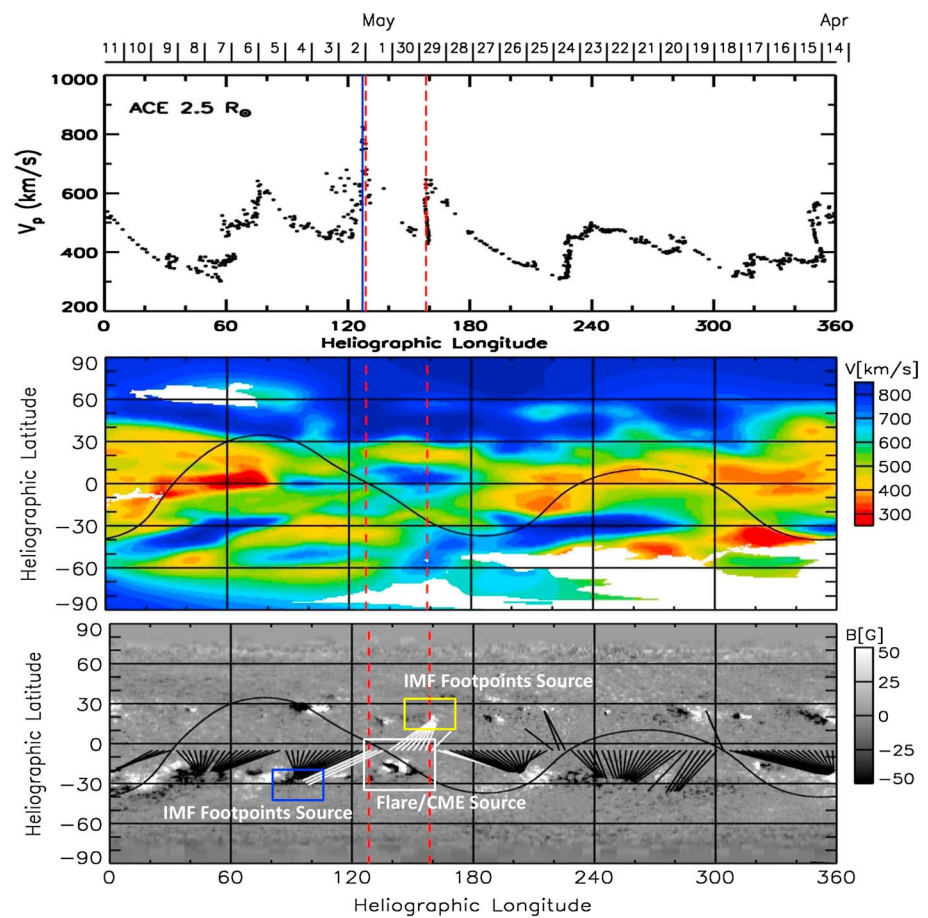


**Figure 6.** (top) ACE measurements of the traced back solar wind velocities to the source surface at  $2.5R_{\odot}$  as function of heliographic longitudes. The vertically oriented red dashed parallel lines indicate the trace back heliographic longitudes of  $128^{\circ}$  and  $158^{\circ}$  corresponding to the prolonged period of southward IMF- $B_z$ , while the vertical blue solid line marks the trace back period corresponds to the onset of SI. Dates of Central Meridian Passage (CMP) are indicated at the top. (middle) A tomographic synoptic velocity map for CR1935, projected onto the source surface at  $2.5R_{\odot}$ , obtained using ISEE IPS data. The curved solid line is the magnetic neutral line. (bottom) A synoptic map for CR1935, made using magnetograms from the MDI instrument on board SOHO. The heliographic longitudes are marked at the bottom of the map. Regions of large magnetic field strength corresponding to active region locations are shown as black and white patches to distinguish the two magnetic polarities, while the curved solid line is the magnetic neutral line. Also shown are converging lines in black which join the potential field computed source surface magnetic fields with their corresponding photospheric footpoints. The converging lines in white correspond to the fields of the CMP date from 29 April to 1 May. The locations of the footpoints on the photosphere are shown inside the rectangular yellow and blue boxes, while the source region of the flare and CME is shown inside a rectangular white box.

It is clear from Figure 6 (middle) that the solar wind flow, in the trace-back region, was largely dominated by velocity flows between  $500$  and  $600 \text{ km s}^{-1}$ . Also, a high-velocity flow was observed north of the equator which is probably an extension of the high-velocity flows from the high-latitude polar coronal holes.

Figure 6 (bottom) shows a synoptic magnetogram during CR1935, from the MDI instrument on board the SOHO spacecraft. The black and white patches represent regions of strong magnetic fields, corresponding to active region locations that distinguish the two opposite magnetic polarities. The curved black line on the map is the source surface MNL, while the two dashed vertical parallel lines bracket the trace back locations. A large active region is seen to be located to the south of the neutral line in the trace back period, which has been identified as the source of the flare and CME that erupted on 29 April and 2 May 1998 [Thompson et al., 2000]. The converging black lines on the synoptic magnetogram join magnetic fields at the source surface to the photosphere. The magnetic fields were computed using a potential field model by Hakamada and Kojima [1999], and they lie in an equally spaced grid along the equator, while their radially back-projected photospheric footpoints lie in tightly bunched regions associated with active regions north and south of the

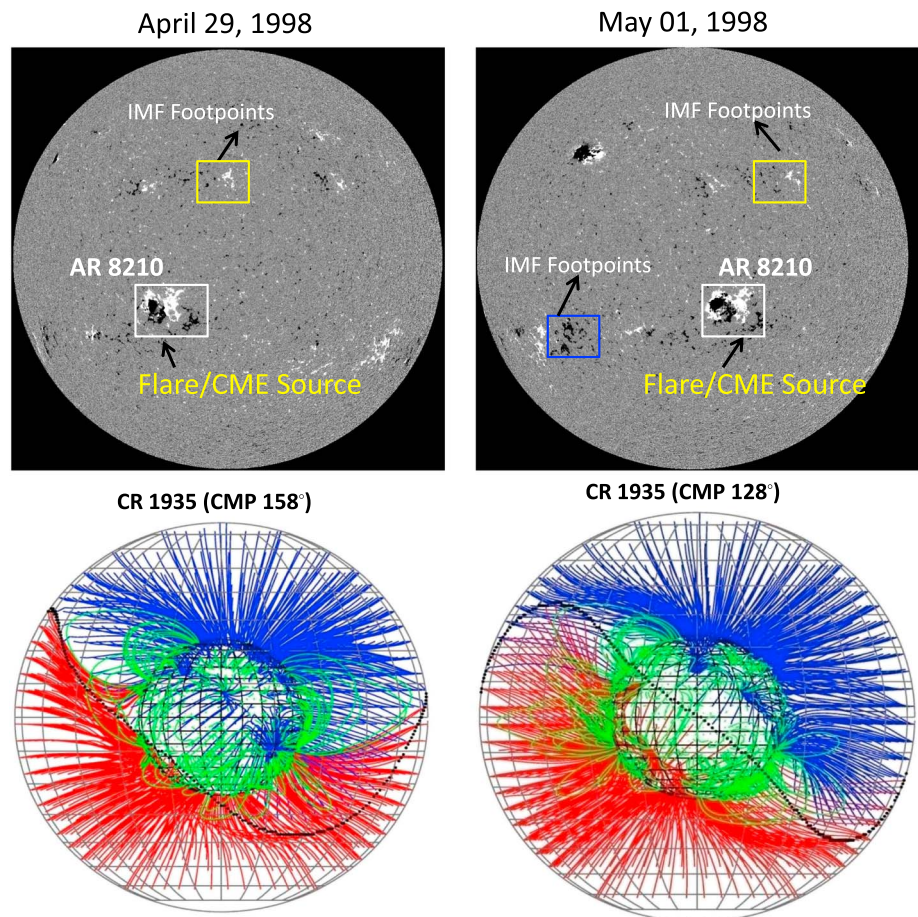


**Figure 7.** Maps of the solar photosphere on (top left) 29 April and (top right) 1 May 1998 are shown, indicating the locations of the source regions. The location of AR 8210 is indicated by a large rectangular white box in both panels, while the IMF footpoint locations are indicated by the small rectangular yellow and blue boxes in both panels. Three-dimensional structure of the coronal magnetic fields for CR1935 on (bottom left) 29 April 1998 and (bottom right) 1 May 1998. The fields were computed using a potential field model and are viewed from  $158^\circ$  (Figure 7, bottom left) and  $128^\circ$  (Figure 7, bottom right) in Carrington longitude. The blue and red lines denote the outward and inward polarities, respectively, and are shown projected on to the source surface at  $2.5R_\odot$ . The green lines denote the close field lines. Only fields between 5 G and 250 G on the photosphere are plotted in order not to clutter the figure. The open field lines at  $2.5 R_\odot$  are plotted in steps of  $5^\circ$  in longitude and latitude.

equator. These footpoints were the source regions of the open magnetic field lines connected from the Sun to 1 AU at the time of event. The lines in white mark the field lines corresponding to the period with CMP dates from 29 April to 1 May 1998. It is important to note that the converging field lines shown in white in Figure 6 (bottom) were found to be associated with active regions both north and south of the equator. The locations of the footpoints on the photosphere are shown inside the rectangular yellow and blue boxes, while the source region of the flare and CME are shown inside a rectangular white box. The magnetic field strength within the pixel areas around the first IMF footpoint location has been found to be weaker, while the field strength around the second IMF footpoint location has been found to be stronger. It is evident Figure 6 (middle) that the region of traced field lines to the north of the equator was dominated by large median velocity flows of approximately  $600\text{--}800\text{ km s}^{-1}$ .

### 6.1. Active Region Locations

Figure 7 (top row) shows the location of active regions on the Sun on 29 April 1998 (top left) and 1 May 1998 (top right). The active region AR 8210, was the source region of the flare/CME that erupted on 29 April, is shown inside a large rectangular white box in Figure 7 (top left). The active region is located close to the central meridian at a longitude of  $16^\circ\text{E}$  to the south of the equator on 29 April. The footpoint of the IMF, at the start of the traced back interval, on 29 April is associated with a small active region shown inside a small

rectangular yellow box in Figure 7 (top left). This active region is located in close proximity to the central meridian on 29 April. Figure 7 (top right) shows the positions of the active regions on 1 May. The location of the IMF footpoint, at the end of the traced back interval, on 1 May is associated with the active region on the south of the equator, shown in a small rectangular blue box.

Figure 7 (bottom row) shows the three-dimensional structure of the computed coronal magnetic fields on 29 April 1998 (bottom left) and 1 May 1998 (bottom right) respectively, as viewed from a Carrington longitude of  $158^\circ$  (bottom left) and  $128^\circ$  (bottom right) corresponding to the start and the end of the traced back interval. The coronal magnetic fields cannot be measured directly and so were computed using photospheric magnetic fields as inputs to potential field extrapolations [Hakamada and Kojima, 1999]. The magnetic field lines from the potential field computations fan out from tightly bunched regions associated with active regions north and south of the equator with the blue and red lines denoting the outward (positive) and inward (negative) open fields, respectively. The green lines denote closed field lines, while the solid black line is the MNL. Only fields between 5 G and 250 G on the photosphere have been plotted in order not to clutter the figure, and the open field lines at  $2.5R_\odot$  are plotted in steps of  $5^\circ$  in longitude and latitude. From Figure 7 (bottom row) it is evident that apart from the polar coronal hole regions showing the open field lines, the other open field lines were associated with the small active region north to the equator, which is the source region of the IMF footpoints of the prolonged southward IMF- $B_z$  interval, as shown inside the small rectangular yellow box in Figure 7 (top left). It is important to note that the open field lines associated with the region were found to be positive and remained constantly north of the MNL both on 29 April and 1 May. This implies that the large-scale open field structures associated with the region did not change their polarity and remained radial beyond the source surface for most of the time during the trace back period corresponding to the prolonged southward IMF event.

It can be seen from Figure 7 (bottom right) that the MNL shifted toward the north-west on 1 May. The open magnetic field structures directed inward were found to the south of the MNL associated with a bunch of closed magnetic field lines and loops. As mentioned earlier, they were the footpoint locations of the traced back IMF at the end of the prolonged southward IMF interval, shown inside a small rectangular blue box in Figure 7 (top right), associated with an active region on the southeast of the solar disk center.

## 7. Discussion

Our analysis of the north-south component of interplanetary magnetic field at 1 AU during geomagnetic storm conditions in the period 2–4 May 1998 showed a nearly 44 h long or unusually prolonged weakly southward IMF- $B_z$  in the time interval from 0920 UT, 2 May 1998 to 0520 UT, 4 May 1998. This is for the first time that such an unusually long duration southward IMF- $B_z$  event has been reported.

### 7.1. Interplanetary Sources

From in situ measurements, at 1 AU, of solar wind plasma and magnetic field, it is evident that the prolonged IMF- $B_z$  event was associated with an ICME identified from 2 May 0500 UT to 4 May 0100 UT. The ICME was actually the counterpart of a large halo CME that erupted on 29 April 1998 at 1658 UT [Thompson *et al.*, 2000; Malandraki *et al.*, 2002]. Prior to the CME eruption, a M6.8 flare erupted at 1606 UT. The shock driven by the flare and CME led to the forward shock at 2123 UT on 1 May and the reverse shock at 0300 UT on 2 May, respectively. The arrival of the forward shock caused the compression of the upstream plasma and led to the fluctuations in the IMF components. Subsequently, the draping of the field lines around the CME in the shocked plasma produced the northward IMF- $B_z$  fields. The arrival of the ICME, marked by a reverse shock, resulted in an out-of-ecliptic IMF component that led to the first southward turning of the IMF- $B_z$ . In a study of the outward propagation of the flare-associated CME, Hoeksema and Zhao [1992] reported the preferential existence of the southward IMF- $B_z$  component at 1 AU. It is, thus, the arrival of the ICME at 1 AU, driven by the flare-associated CME of 29 April that led to the first southward turning of the IMF- $B_z$  observed at 0920 UT on 2 May.

The ICME interval at 1 AU contained a well-defined MC observed from 1300 UT, 2 May to 1200 UT, 3 May, for over 24 h. Given such long hours of traversal of MC, we estimated the radial width of the MC and found it to be nearly 0.28 AU. Also, in situ observation of the monotonic decreases in the solar wind speed, and the magnitude of the magnetic field shows that the MC was expanding in the IP space. As mentioned earlier, it has been reported by Malandraki *et al.* [2002] that the magnetic field lines during the ICME passage were

anchored to the Sun. Also, as discussed above, the fields were already southward, prior to the MC, due to the arrival of the ICME. Thus, as the MC approached, the southward field lines draped around the MC and led them to be farther southward and intense [Gonzalez *et al.*, 1994]. Since the source region of the CME that erupted on 29 April was in the south of the disk center, the internal field of the CME/MC should have a southward directed field [McComas *et al.*, 1989]. It is known that most MCs while propagating through the IP space do not change their polarity [Marubashi, 1986], so the southward directed internal field could result in a southward IMF component at 1 AU. Earlier observations [Zhao and Hoeksema, 1998; Zhang and Moldwin, 2014] have also reported that the most southward IMF- $B_z$  events are associated with ICME having MC signatures. It is, thus, expected that the prolonged weakly southward magnetic fields, for nearly 24 h, during 3 May was a result of the expanding large MC associated with the ICME passage. Also, the long duration of MC can be studied by comparing the magnetic flux geometry of the MC at the location of the encounter with the spacecraft, obtained using the magnetic flux rope models [Burlaga, 1988; Marubashi, 2000; Marubashi and Lepping, 2007; Marubashi *et al.*, 2015], to the observed magnetic field variations at 1 AU.

The arrival of a second forward shock and an IP discontinuity at 1 AU [Skoug *et al.*, 1999], driven by a second flare-associated CME erupted on 2 May 1406 UT [Skoug *et al.*, 1999; Malandraki *et al.*, 2002], compressed the preexisting southward IMF- $B_z$  component [Tsurutani *et al.*, 1988; Gonzalez *et al.*, 1994]. This, in turn, resulted in a strong southward IMF- $B_z$  as noticed on 4 May 0200 UT.

## 7.2. Solar Sources

Two flare-associated CMEs erupted, respectively, on 29 April and 2 May. The source region of both of the CMEs was a large active region AR 8210 [Thompson *et al.*, 2000]. We tracked source regions of the solar wind flows associated with the event, using the trace back technique of constant velocities along Archimedean spirals, back to the solar source surface at  $2.5R_{\odot}$ . The source locations of solar wind flows, corresponding to the start and the end of the IMF interval, were identified to the south of the equator and between the heliographic longitudes of  $128^{\circ}$  and  $158^{\circ}$ . From observations of solar wind velocity from ISEE/IPS observatory and the photospheric magnetic fields from SOHO/MDI, we were able to show that the traced back flows were associated with an active region AR 8210 at a longitude of  $16^{\circ}$ S. It is to be noted that the active region is the source region of the flares/CMEs that erupted on 29 April and 2 May. A positive SI was observed at the end of the present long duration southward IMF event. This was caused due to a shock driven by a second faster CME, which erupted on 2 May, and arrived behind the first CME just prior to the end of the first ICME interval. The arrival of the second shock just before the end of the first ICME raised the question whether the eruption of the second CME had destroyed the magnetic configuration of the field lines during the trace back period, and whether information of the background IMF conditions on the solar surface was destroyed. From our analysis, however, we showed that the eruption of CME took place right after our trace back period, indicating that the source regions of the IMF determined by the velocity trace back technique would be valid [Ko *et al.*, 2013]. It is also to be noted that the active region AR 8210 remained south of the magnetic neutral line (MNL) during the whole trace back period, indicating no change in the IMF configuration.

Using the field line tracing of the computed coronal magnetic fields from the solar surface to the photosphere, we were able to locate the footpoints of the IMF source region at the start of the prolonged southward IMF- $B_z$  event at 1 AU to a small unnamed active region on 29 April, lying close to the central meridian and to the north of the equator. The footpoints of the IMF source regions at the end of the prolonged southward IMF- $B_z$  event at 1 AU were found to be associated with a region in the close proximity of an active region, located to the south of the equator. The magnetic field lines during the passage of the ICME were anchored to the Sun; thus, the footpoints of the traced back IMF were actually the foot regions of the ICME observed at 1 AU. Further, the potential field computations of source surface magnetic fields on 29 April and 1 May showed open magnetic field structures with positive polarity emanating from this unnamed active region. The open field lines, which remained constantly to the north of the heliospheric current sheet both on 29 April and 1 May, clearly suggest no change in their polarity during the trace back period, from 29 April to 1 May. It is also known from observations that, depending on the hemisphere, the open magnetic field lines spiral either inward or outward, and the configuration changes, generally, either during periodic solar polar reversals occurring at the maximum of each solar cycle [Janardhan *et al.*, 2005, 2008a, 2008b] or due to the wake of CME eruption [Ko *et al.*, 2013]. However, the polarity reversal of solar cycle 23 occurred in CR1949, while our event was during CR1935. Also, the second CME was erupted on 2 May, after our trace back period and after the first CME which erupted on 29 April. From our observations, it is evident that the sudden change in proton velocity (due to the eruption of the CME on 29 April) was seen before or around the same period when the

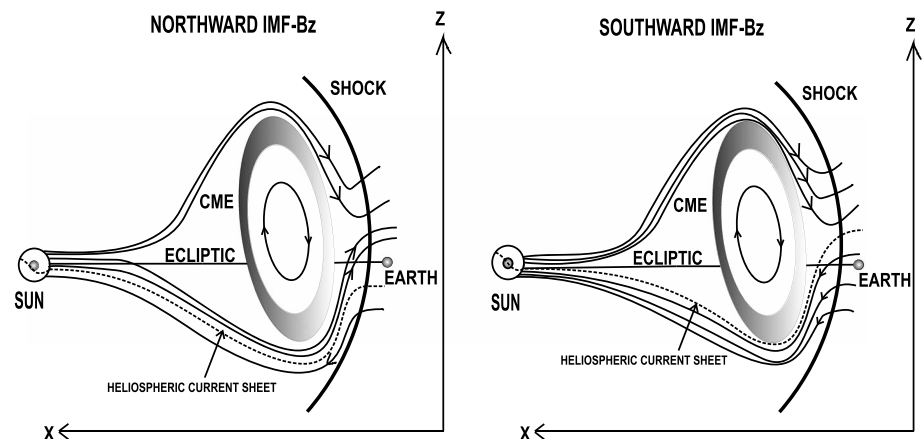


**Figure 8.** A schematic showing the draping of the field lines around the CME in the IP space. (left) The CME of 29 April propagating in the north of the ecliptic led to the draping of the field lines in the shocked plasma, which were directed outward, and generated the northward IMF- $B_z$  fields at 1 AU. (right) The CME of 2 May propagating in the north of the ecliptic led to the draping of the field lines in the shocked plasma, which were directed inward (sunward) and generated the southward IMF- $B_z$  fields at 1 AU. Both the CME had southward directed internal fields as their source regions were located to the south of the solar disk. The position of the HCS on the Sun and in the IP space has been shown by a dotted line. The HCS separates the positive and negative IMF field lines.

IMF- $B_z$  at 1 AU became southward. Therefore, no change in magnetic field configuration can be expected. It is noticed, however, from our field line tracing that the IMF showed a change, toward the end of the southward IMF- $B_z$  interval, in their footpoint locations from the north to the south. Also, the potential field computations of source surface magnetic fields on 1 May showed open magnetic field lines with negative polarity emanating close to the southeast active region. This is consistent with observation of the IMF crossing at 1 AU (change in the value of  $\phi$  from positive to negative as shown in Figure 2) during the ICME passage.

Figure 8 shows a schematic of the draping of the field lines around the CME plasma. As mentioned earlier, the first CME, erupted on 29 April, was propagating northward [Wang *et al.*, 2000], so the center of the CME would be to the north of the ecliptic. Also, the IMF field lines were directed away from the Sun (outward), while the HCS was to the south of the equator. Such a condition with the CME propagating to the north of the ecliptic and with the field lines radially outward has been shown in Figure 8 (left). It can be seen from Figure 8 that the draping of the field lines around the CME, in the shocked plasma, has resulted in northward IMF- $B_z$  fields [Gosling and McComas, 1987; McComas *et al.*, 1989]. This is consistent with the observed northward IMF- $B_z$  fields noticed after the postshock early on 2 May. The CME internal field, which was southward directed, resulted in the southward IMF- $B_z$  fields at 1 AU. The second CME, erupted on 2 May, was also propagating to the north [Wang *et al.*, 2002], so the center of the CME would be to the north of the ecliptic. The IMF field lines, as mentioned earlier, on the north were still radially outward, while the IMF field lines on the south were radially inward. As mentioned earlier, the HCS moved to the northwest but was still to the south of the equator. Figure 8 (right) presents such a condition, where the CME was propagating to the north of the ecliptic and the field lines were radially inward, which resulted in southward IMF- $B_z$  fields due to the draping of the sunward field lines around the CME/MC. The southward fields when approached the MC within the CME having southward directed internal fields would be intensified further. In fact, strong southward IMF- $B_z$  fields were observed toward the end of the interval. Assuming the CME moved radially outward from the Sun, the IMF fields originally anchored to the Sun southward (northward) of the CME source location would still be traced back to the Sun southward (northward) of the CME [McComas *et al.*, 1989]. It is to be noted that the CMEs of 29 April and 2 May erupted from the same active region, AR 8210, which was located to the south of the disk center. Thus, when we tracked down the radial IMF fields at the start and the end of the interval, the IMF footpoints were located to the north and the south of the equator, respectively, as expected.

It is, thus, clear that the passage of the ICMEs in the interplanetary medium played a crucial role that led to the unusually prolonged southward IMF- $B_z$  condition. The open field lines from the northern active region, which were anchored to the Sun and remained constantly radially outward during the whole interval, explained the observed polarity changes of the IMF- $B_z$  fields within the shocked plasma.

### 7.3. Geomagnetic Activity

The IMF- $B_z$  remaining southward for a prolonged of 44 hours during 2–4 May led to a moderate storm and a strong storm early on 2 May and early on 4 May, respectively. In between the storms during the weakly prolonged quasi-stable IMF- $B_z$  condition ( $B_z \geq -5$  nT) on 3 May, we also found multiple peaks in the *SYM-H* with corresponding enhancements in the solar wind dynamic pressure (and solar wind density) between 0700 UT and 1700 UT on 3 May 1998. These pulses are unique in a sense that both the IMF- $B_z$  and solar wind velocity barely showed any variation. Thus, any significant change in the ground level magnetic fields could be attributed to the solar wind pressure variations (or density variations). The multiple peaks identified both at low-latitude Indian stations and 210 MM network of stations during the above period provided a clear evidence that these enhancements were global in nature. Since perturbations in *SYM-H* index, usually represent mean variations in the symmetric ring current (the westward symmetric electric current that flows along the geomagnetic equator), it is clear that the prolonged weakly southward IMF- $B_z$  preconditions on 2–4 May 1998 developed a quasi-stable ring current, promoted by solar wind-magnetosphere coupling for a long period.

In the presence of the strong southward IMF- $B_z$  for long intervals, the solar wind flux has been continuously loaded to the magnetosphere/magnetotail causing a magnetospheric convection on the nightside. This, in turn, leads to transport and acceleration of particles from the magnetotail and the plasma sheet toward the Earth's inner magnetosphere [Kamide *et al.*, 1998; Daglis *et al.*, 1999] forming the storm-time ring current. In the present study, early on 2 May, when the southward IMF- $B_z$  was relatively stronger, the ring current was intensified, as seen by the relative depression in *SYM-H* index, due to the enhanced convection. Early on 3 May while the southward IMF- $B_z$  was relatively weaker, it is not expected to form a ring current. Under these weak IMF- $B_z$  conditions, the density variations in the solar wind can be a driver for the ring current [Chen *et al.*, 1994; Jordanova *et al.*, 1998; Borovsky *et al.*, 1998; Smith *et al.*, 1999; Wang *et al.*, 2003]. The plasma sheet density in the near-Earth plasma sheet regions, which is well correlated to the density in the solar wind [Terasawa *et al.*, 1997; Borovsky *et al.*, 1997, 1998], supplies the energy and forms the ring current [Thomsen *et al.*, 1998; Kozyra *et al.*, 1998; Liemohn *et al.*, 1999]. In the present case, the increases in the solar wind density, from 10 to 60 cm<sup>-3</sup> early on 3 May, when the IMF- $B_z$  was weak but still southward, perhaps led to increased number of particles entering the magnetosphere. This, in turn, increased the energy accumulated in the magnetotail and plasma sheet, even when the energy injection began to decline due to the saturated magnetospheric convection. Subsequently, the solar wind dynamic pressure enhancements, corresponding to density variations during 0700–1700 UT on 3 May, formed a quasi-stable ring current. We believe that the multiple peaks in the *SYM-H* index were manifestations of the multiple peaks developed in the quasi-stable ring current. Our study, thus, indicates that  $P_{\text{dyn}}$  variations owing to density changes might play an important role in the development of ring current during the quasi-steady prolonged southward IMF- $B_z$  condition. In a similar study, Araki *et al.* [1993] showed the effect of the solar wind dynamic pressure, caused by solar wind density variations, on the geomagnetic field through study of changes in the *Dst* index. The study [Tanskanen *et al.*, 2005] of the solar wind preconditions during the different magnetotail phenomena corresponding to the prolonged southward IMF- $B_z$  intervals reported that the magnetospheric convection is more likely when the mean southward IMF- $B_z$  is  $\geq -5$  nT, while loading and unloading are more likely when IMF- $B_z$  is  $\leq -5$  nT. In the present study, we found that the southward IMF- $B_z$  was  $\geq -5$  nT during the weakly southward IMF- $B_z$  condition on 3 May. It indicates an occurrence of a nightside steady magnetospheric convection during the period which, thus, led to the development of a quasi-stable ring current owing to the density variations.

Also, our periodogram analysis suggested the presence of the discrete frequencies in the solar wind density variations, during 0700–1700 UT, 3 May, near  $f = 0.48, 0.65,$  and  $0.75$  mHz or  $T = 35, 26,$  and  $22$  min. It is known from earlier observations [Kepko *et al.*, 2002; Kepko and Spence, 2003; Viall *et al.*, 2009a] that such long period and sub-mHz ULF oscillations have been existed in magnetospheric fields. Confirming the fact, we also found the similar discrete frequencies in the ground magnetic fields or the symmetric ring current strength (*SYM-H* fields). The frequencies obtained here in solar wind density variations are in agreement with those reported by Viall *et al.* [2009a]. Also, the estimation of their radial length scales showed that the associated PDS of the density variations have significant power at wavelengths,  $L = 600, 704, 756, 947,$  and  $1160$  Mm. The observed length scales of the PDS estimated here are larger in sizes than those reported by Viall *et al.* [2008]. Our spectral analysis results fit well into the global picture that shows that the ULF oscillations of the solar wind density variations act as the drivers of the magnetospheric field oscillations. The density variations could be attributed to the significantly increased values of the He<sup>++</sup>/H<sup>+</sup> ratio [Skoug *et al.*, 1999] observed at 1 AU, between 1800 UT on 2 May and 1700 UT on 3 May, though the origin of the density pulses needs to be

investigated. The origin of the associated PDS with the density variations has been well studied [Viall *et al.*, 2009b, 2010; Viall and Vourlidas, 2015], which revealed that these can be due to variations in the solar coronal plasma, which convect with the ambient solar wind from the Sun to 1 AU. The increased  $\text{He}^{++}/\text{H}^+$  ratio at 1 AU, during the prolonged southward IMF- $B_z$  interval, indicates that the PDS could be of the solar origin, which convected with the solar wind during the outward propagation of the CME from the Sun to 1 AU [Viall *et al.*, 2009b]. The details of those, however, require a separate further study and will be investigated in a future work.

It is generally understood that the Earth's magnetotail during such long hours of the southward IMF- $B_z$  intervals respond in different manners such as isolated loading and unloading, periodic loading and unloading, and steady magnetospheric convection [Tanskanen *et al.*, 2005, and references therein]. A series of substorms, known as periodic substorms, can occur when the southward IMF- $B_z$  is southward for several hours [Huang, 2002; Huang *et al.*, 2003a, 2003b]. Since the magnetosphere is open for long hours during these IMF- $B_z$  conditions, solar wind variations can make their way into the magnetosphere and subsequently to the ground causing disturbances at low latitude and mid latitude with periods of nearly 2–3 h. These substorms are usually associated with periodic loading and unloading of plasma particle fluxes and are commonly referred to as saw tooth events [Henderson, 2004]. They, in turn, can contribute to disturbances recorded at ground magnetic stations. Thus, one of the possible reasons for the occurrence of the multiple pulses on 3 May 1998 may be due to the substorm activity. So it is important to delineate the multiple processes occurring together. We have taken care to verify the energetic proton fluxes from all the available Los Alamos National Laboratory (LANL) spacecraft to see if there were any periodic injections of fluxes. However, except for the pulse  $P_3$ , we did not find such flux injections corresponding to the onset of pulses  $P_1$ ,  $P_2$ , and  $P_4$ , rejecting the possibility of any periodic substorms during that period.

Besides the precursor southward IMF of more than 10 h, typical signatures of magnetospheric/magnetotail preconditioning were found prior to the onset of the storm on 4 May such as a SI, constant values of  $\text{SYM-H}$  with  $\leq -50$  nT, and a fairly constant substorm activity with the values of  $AE$  between 500 and 1000 nT. The great storms reported by Tsurutani *et al.* [1992] also showed similar magnetospheric/magnetotail preconditioning with  $Dst \leq -50$  nT and  $AE \geq 500$  nT prior to the onset of the great magnetic storm. However, a careful inspection of the  $AE$  and  $AL$  indices, in the present study, with  $AE \geq -2500$  nT showed that they were not supersubstorms as discussed in Tsurutani *et al.* [2015].

## 8. Summary and Conclusion

The present work is important as it is for the first time such a prolonged weakly southward IMF- $B_z$  of nearly 44 h has been reported, and the cause of this has been addressed in detail by investigating both the interplanetary and solar sources. The interplanetary plasma and magnetic field measurements at 1 AU showed the passage of two ICMEs during the event. The shocks and the magnetic cloud driven by the first ICME led to the observed southward IMF- $B_z$  during 2–4 May. The sharp southward IMF- $B_z$  near the end of the event was due to the second ICME and its upstream shock. Investigation of the solar sources indicated that the first ICME was due to a fast halo CME which erupted on 29 April and the second ICME was due to a fast halo CME erupted on 2 May. It is to be noted that both the CMEs erupted from the same active region AR 8210.

Also, we were able to locate the source region of the solar wind flows and the associated IMF during the event to the solar surface at  $2.5R_{\odot}$ , located in close proximity of the active region AR 8210. The field line tracing of the IMF, from the source surface to the photosphere, showed that the footpoints of the IMF during the event were associated with a small active region on the north and an active region on the south of the equator. Examination of their corresponding magnetic configuration showed open magnetic field structures emanating from the northern active region. These open field lines were directed away from the Sun and did not change their direction during the whole trace back period of 29 April to 1 May, corresponding to the event at 1 AU. The draping of these constantly radial outward field lines, during the prolonged southward IMF- $B_z$  interval, around the CME/MC at 1 AU, explains the observed polarity changes of the IMF- $B_z$  within the shocked plasma.

Additionally, we also investigated multiple global disturbances of the geomagnetic fields from 0700 to 1700 UT on 3 May to understand the underlying cause. It was shown that the multiple density enhancements in the solar wind, within a period of only 10 h, could develop quasi-stable ring currents. This, in turn, could lead to the multiple surface magnetic field deviations, without the contribution from either the solar wind velocity or the IMF- $B_z$ . Further, the spectral analyses of solar wind density and geomagnetic field variations showed the

presence of the common discrete frequencies at 0.48, 0.65, and 0.75 mHz confirming the solar wind density variations as the driver of the global geomagnetic disturbances. The work, thus, presents an observational link of solar surface phenomena with that of worldwide magnetic response during an unusually prolonged southward IMF- $B_z$  condition.

### Acknowledgments

The authors thank J.H. King and N. Papatashvili of Adnet Systems, NASA, GSFC, the CDAWeb team, the ACE instrument team, the ACE Science Center, and the MDI consortia for making data available in the public domain via the World Wide Web. SOHO is a project of international collaboration between ESA and NASA. IPS observations were carried out under the solar wind program of ISEE, Nagoya University, Japan. For IMF and solar wind data used can be obtained from <http://cdaweb.gsfc.nasa.gov/cgi-bin/eval2.cgi>. ACE and MDI/SOHO data are available in the public domain (<http://www.srl.caltech.edu/ACE/ASC/level2/index.html> and [http://sohodata.nascom.nasa.gov/cgi-bin/data\\_query](http://sohodata.nascom.nasa.gov/cgi-bin/data_query)). Other data are available from the authors upon request such as for IPS solar wind velocity ([fujiki@stelab.nagoya-u.ac.jp](mailto:fujiki@stelab.nagoya-u.ac.jp)), Indian magnetograms used in the present paper ([susanta@nao.cas.cn](mailto:susanta@nao.cas.cn)), and 210 MM magnetograms ([yoshi@geo.kyushu-u.ac.jp](mailto:yoshi@geo.kyushu-u.ac.jp)). S.K.B. acknowledges the support by the Chinese Academy of Sciences International Talent Scheme, project 2015PM066 (Funded by Chinese Academy of Sciences President's International Fellowship Initiative). Yihua Yan is supported by NSFC grant 11433006. The work by A.Y. was supported by MEXT/JSPS KAKENHI grant15H05815. One of the authors, J.P., would like to thank U.R. Rao for useful suggestions that have improved the paper. The authors also thank the reviewers for their constructive comments and suggestions that have significantly improved the paper.

### References

- Ananthakrishnan, S., V. Balasubramanian, and P. Janardhan (1995), Latitudinal variation of solar wind velocity, *Space Sci. Rev.*, *72*, 229–232, doi:10.1007/BF00768784.
- Araki, T., K. Funato, T. Iguchi, and T. Kamei (1993), Direct detection of solar wind dynamic pressure effect on ground geomagnetic field, *Geophys. Res. Lett.*, *20*, 775–778, doi:10.1029/93GL00852.
- Bagiya, M. S., R. Hazarika, F. I. Laskar, S. Sunda, S. Gurubaran, D. Chakrabarty, P. K. Bhuyan, R. Sridharan, B. Veenadhari, and D. Pallamraju (2014), Effects of prolonged southward interplanetary magnetic field on low-latitude ionospheric electron density, *J. Geophys. Res. Space Physics*, *119*, 5764–5776, doi:10.1002/2014JA020156.
- Balasubramanian, V., P. Janardhan, S. Srinivasan, and S. Ananthakrishnan (2003), Interplanetary scintillation observations of the solar wind disappearance event of May 1999, *J. Geophys. Res.*, *108*, 1121, doi:10.1029/2002JA009516.
- Bamert, K., R. F. Wimmer-Schweingruber, R. Kallenbach, M. Hilchenbach, B. Klecker, A. Bogdanov, and P. Wurz (2002), Origin of the May 1998 suprathermal particles: Solar and heliospheric observatory/charge, element, and isotope analysis system/(highly) suprathermal time of flight results, *J. Geophys. Res.*, *107*, 1130, doi:10.1029/2001JA900173.
- Bisoi, S. K., P. Janardhan, M. Ingale, P. Subramanian, S. Ananthakrishnan, M. Tokumar, and K. Fujiki (2014a), A study of density modulation index in the inner heliospheric solar wind during solar cycle 23, *Astrophys. J.*, *795*, 69, doi:10.1088/0004-637X/795/1/69.
- Bisoi, S. K., P. Janardhan, D. Chakrabarty, S. Ananthakrishnan, and A. Divekar (2014b), Changes in quasi-periodic variations of solar photospheric fields: Precursor to the deep solar minimum in cycle 23?, *Sol. Phys.*, *289*, 41–61, doi:10.1007/s11207-013-0335-3.
- Borovsky, J. E., M. F. Thomsen, and D. J. McComas (1997), The superdense plasma sheet: Plasmaspheric origin, solar wind origin, or ionospheric origin?, *J. Geophys. Res.*, *102*, 22,089–22,106, doi:10.1029/96JA02469.
- Borovsky, J. E., M. F. Thomsen, and R. C. Elphic (1998), The driving of the plasma sheet by the solar wind, *J. Geophys. Res.*, *103*, 17,617–17,640, doi:10.1029/97JA02986.
- Brueckner, G. E., et al. (1995), The large angle spectroscopic coronagraph (LASCO), *Sol. Phys.*, *162*, 357–402, doi:10.1007/BF00733434.
- Bruno, R., L. F. Burlaga, and A. J. Hundhausen (1982), Quadrupole distortions of the heliospheric current sheet in 1976 and 1977, *J. Geophys. Res.*, *87*, 10,339–10,346, doi:10.1029/JA087iA12p10339.
- Bruno, R., L. F. Burlaga, and A. J. Hundhausen (1984), K-coronameter observations and potential field model comparison in 1976 and 1977, *J. Geophys. Res.*, *89*, 5381–5385, doi:10.1029/JA089iA07p05381.
- Burlaga, L., E. Sittler, F. Mariani, and R. Schwenn (1981), Magnetic loop behind an interplanetary shock—Voyager, Helios, and IMP 8 observations, *J. Geophys. Res.*, *86*, 6673–6684, doi:10.1029/JA086iA08p06673.
- Burlaga, L. F. (1988), Magnetic clouds and force-free fields with constant alpha, *J. Geophys. Res.*, *93*, 7217–7224, doi:10.1029/JA093iA07p07217.
- Chen, J., and T. A. Fritz (1999), May 4, 1998 storm: Observations of energetic ion composition by POLAR, *Geophys. Res. Lett.*, *26*, 2921–2924, doi:10.1029/1999GL003582.
- Chen, J., and T. A. Fritz (2001), Features of energetic ions near the compressed magnetosphere, *J. Atmos. Sol. Terr. Phys.*, *63*, 463–472, doi:10.1016/S1364-6826(00)00173-5.
- Chen, M. W., L. R. Lyons, and M. Schulz (1994), Simulations of phase space distributions of storm time proton ring current, *J. Geophys. Res.*, *99*, 5745–5759, doi:10.1029/93JA02771.
- Daglis, I. A., R. M. Thorne, W. Baumjohann, and S. Orsini (1999), The terrestrial ring current: Origin, formation, and decay, *Rev. Geophys.*, *37*, 407–438, doi:10.1029/1999RG900009.
- Domingo, V., B. Fleck, and A. I. Poland (1995), The SOHO mission: An overview, *Sol. Phys.*, *162*, 1–2, doi:10.1007/BF00733425.
- Dungey, J. W. (1961), Interplanetary magnetic field and the auroral zones, *Phys. Rev. Lett.*, *6*, 47–48, doi:10.1103/PhysRevLett.6.47.
- Echer, E., W. D. Gonzalez, B. T. Tsurutani, and A. L. C. Gonzalez (2008a), Interplanetary conditions causing intense geomagnetic storms ( $Dst < -100$  nT) during solar cycle 23 (1996–2006), *J. Geophys. Res.*, *113*, A05221, doi:10.1029/2007JA012744.
- Echer, E., W. D. Gonzalez, and B. T. Tsurutani (2008b), Interplanetary conditions leading to superintense geomagnetic storms ( $Dst < -250$  nT) during solar cycle 23, *Geophys. Res. Lett.*, *35*, L06S03, doi:10.1029/2007GL031755.
- Francia, P., S. Lepidi, P. D. Giuseppe, and U. Villante (2001), Geomagnetic sudden impulses at low latitude during northward interplanetary magnetic field conditions, *J. Geophys. Res.*, *106*, 21,231–21,236, doi:10.1029/2000JA900136.
- Ganushkina, N. Y., T. I. Pulkkinen, and T. Fritz (2005), Role of substorm-associated impulsive electric fields in the ring current development during storms, *Ann. Geophys.*, *23*, 579–591, doi:10.5194/angeo-23-579-2005.
- Gloeckler, G., L. A. Fisk, S. Hefti, N. A. Schwadron, T. H. Zurbuchen, F. M. Ipavich, J. Geiss, P. Bochsler, and R. F. Wimmer-Schweingruber (1999), Unusual composition of the solar wind in the 2–3 May 1998 CME observed with SWICS on ACE, *Geophys. Res. Lett.*, *26*, 157–160, doi:10.1029/1998GL900166.
- Gonzalez, W. D., and B. T. Tsurutani (1987), Criteria of interplanetary parameters causing intense magnetic storms ( $Dst$  of less than  $-100$  nT), *Planet. Space Sci.*, *35*, 1101–1109, doi:10.1016/0032-0633(87)90015-8.
- Gonzalez, W. D., J. A. Joselyn, Y. Kamide, H. W. Kroehl, G. Rostoker, B. T. Tsurutani, and V. M. Vasyliunas (1994), What is a geomagnetic storm?, *J. Geophys. Res.*, *99*, 5771–5792, doi:10.1029/93JA02867.
- Gosling, J. T., and D. J. McComas (1987), Field line draping about fast coronal mass ejecta—A source of strong out-of-the-ecliptic interplanetary magnetic fields, *Geophys. Res. Lett.*, *14*, 355–358, doi:10.1029/GL014i004p00355.
- Gosling, J. T., E. Hildner, R. M. MacQueen, R. H. Munro, A. I. Poland, and C. L. Ross (1974), Mass ejections from the Sun—A view from SKYLAB, *J. Geophys. Res.*, *79*, 4581–4587, doi:10.1029/JA079i031p04581.
- Gosling, J. T., S. J. Bame, D. J. McComas, and J. L. Phillips (1990), Coronal mass ejections and large geomagnetic storms, *Geophys. Res. Lett.*, *17*, 901–904, doi:10.1029/GL017i007p00901.
- Hakamada, K., and M. Kojima (1999), Solar wind speed and expansion rate of the coronal magnetic field during Carrington rotation 1909, *Sol. Phys.*, *187*, 115–122, doi:10.1023/A:1005183914772.
- Henderson, M. G. (2004), The May 2–3, 1986 CDAW-9C interval: A sawtooth event, *Geophys. Res. Lett.*, *31*, L11804, doi:10.1029/2004GL019941.

- Hewish, A., P. F. Scott, and D. Wills (1964), Interplanetary scintillation of small diameter radio sources, *Nature*, *203*, 1214–1217, doi:10.1038/2031214a0.
- Hoeksema, J. T., and X. Zhao (1992), Prediction of magnetic orientation in driver gas associated -Bz events, *J. Geophys. Res.*, *97*, 3151–3157, doi:10.1029/91JA02702.
- Huang, C., Y. Yan, G. Li, Y. Deng, and B. Tan (2014), Tracking back the solar wind to its photospheric footpoints from wind observations—A Statistical Study, *Sol. Phys.*, *289*, 3109–3119, doi:10.1007/s11207-014-0508-8.
- Huang, C.-S. (2002), Evidence of periodic (2–3 hour) near-tail magnetic reconnection and plasmoid formation: Geotail observations, *Geophys. Res. Lett.*, *29*, 2189, doi:10.1029/2002GL016162.
- Huang, C.-S., G. D. Reeves, J. E. Borovsky, R. M. Skoug, Z. Y. Pu, and G. Le (2003a), Periodic magnetospheric substorms and their relationship with solar wind variations, *J. Geophys. Res.*, *108*, 1255, doi:10.1029/2002JA009704.
- Huang, C.-S., J. C. Foster, G. D. Reeves, G. Le, H. U. Frey, C. J. Pollock, and J.-M. Jahn (2003b), Periodic magnetospheric substorms: Multiple space-based and ground-based instrumental observations, *J. Geophys. Res.*, *108*, 1411, doi:10.1029/2003JA009992.
- Iju, T., S. Abe, M. Tokumaru, and K. Fujiki (2015), Plasma distribution of Comet ISON (C/2012 S1) observed using the radio scintillation method, *Icarus*, *252*, 301–310, doi:10.1016/j.icarus.2015.02.007.
- Illing, R. M. E., and A. J. Hundhausen (1986), Disruption of a coronal streamer by an eruptive prominence and coronal mass ejection, *J. Geophys. Res.*, *91*, 10,951–10,960, doi:10.1029/JA091iA10p10951.
- Janardhan, P., and S. K. Alurkar (1993), Angular source size measurements and interstellar scattering at 103 MHz using interplanetary scintillation, *Astron. Astrophys.*, *269*, 119–127.
- Janardhan, P., S. K. Alurkar, A. D. Bobra, and O. B. Slee (1991), Enhanced radio source scintillation due to comet Austin 1989C1, *Aust. J. Phys.*, *44*, 565.
- Janardhan, P., S. K. Alurkar, A. D. Bobra, O. B. Slee, and D. Waldron (1992), Power spectral analysis of enhanced scintillation of quasar 3C459 due to Comet Halley, *Aust. J. Phys.*, *45*, 115–126.
- Janardhan, P., V. Balasubramanian, S. Ananthkrishnan, M. Dryer, A. Bhatnagar, and P. S. McIntosh (1996), Travelling interplanetary disturbances detected using interplanetary scintillation at 327 MHz, *Sol. Phys.*, *166*, 379–401, doi:10.1007/BF00149405.
- Janardhan, P., K. Fujiki, M. Kojima, M. Tokumaru, and K. Hakamada (2005), Resolving the enigmatic solar wind disappearance event of 11 May 1999, *J. Geophys. Res.*, *110*, A08101, doi:10.1029/2004JA010535.
- Janardhan, P., K. Fujiki, H. S. Sawant, M. Kojima, K. Hakamada, and R. Krishnan (2008a), Source regions of solar wind disappearance events, *J. Geophys. Res.*, *113*, A03102, doi:10.1029/2007JA012608.
- Janardhan, P., D. Tripathi, and H. E. Mason (2008b), The solar wind disappearance event of 11 May 1999: Source region evolution, *Astron. Astrophys. Lett.*, *488*, L1–L4, doi:10.1051/0004-6361/200809667.
- Jordanova, V. K., C. J. Farrugia, L. Janoo, J. M. Quinn, R. B. Torbert, K. W. Ogilvie, R. P. Lepping, J. T. Steinberg, D. J. McComas, and R. D. Belian (1998), October 1995 magnetic cloud and accompanying storm activity: Ring current evolution, *J. Geophys. Res.*, *103*, 79–92, doi:10.1029/97JA02367.
- Kamide, Y., et al. (1998), Current understanding of magnetic storms: Storm-substorm relationships, *J. Geophys. Res.*, *103*, 17,705–17,728, doi:10.1029/98JA01426.
- Kepko, L., and H. E. Spence (2003), Observations of discrete, global magnetospheric oscillations directly driven by solar wind density variations, *J. Geophys. Res.*, *108*, 1257, doi:10.1029/2002JA009676.
- Kepko, L., H. E. Spence, and H. J. Singer (2002), ULF waves in the solar wind as direct drivers of magnetospheric pulsations, *Geophys. Res. Lett.*, *29*, 1197, doi:10.1029/2001GL014405.
- Klein, L. W., and L. F. Burlaga (1982), Interplanetary magnetic clouds at 1 AU, *J. Geophys. Res.*, *87*, 613–624, doi:10.1029/JA087iA02p00613.
- Ko, Y.-K., A. J. Tylka, C. K. Ng, Y.-M. Wang, and W. F. Dietrich (2013), Source regions of the interplanetary magnetic field and variability in heavy-ion elemental composition in gradual solar energetic particle events, *Astrophys. J.*, *776*, 92, doi:10.1088/0004-637X/776/2/92.
- Kojima, M., and T. Kakinuma (1990), Solar cycle dependence of global distribution of solar wind speed, *Space Sci. Rev.*, *53*, 173–222, doi:10.1007/BF00212754.
- Kojima, M., M. Tokumaru, H. Watanabe, A. Yokobe, K. Asai, B. V. Jackson, and P. L. Hick (1998), Heliospheric tomography using interplanetary scintillation observations 2. Latitude and heliocentric distance dependence of solar wind structure at 0.1–1 AU, *J. Geophys. Res.*, *103*, 1981–1990, doi:10.1029/97JA02162.
- Kozyra, J. U., V. K. Jordanova, J. E. Borovsky, M. F. Thomsen, D. J. Knipp, D. S. Evans, D. J. McComas, and T. E. Cayton (1998), Effects of a high-density plasma sheet on ring current development during the November 2–6, 1993, magnetic storm, *J. Geophys. Res.*, *103*, 26,285–26,306, doi:10.1029/98JA01964.
- Kozyra, J. U., et al. (2014), Solar filament impact on 21 January 2005: Geospace consequences, *J. Geophys. Res. Space Physics*, *119*, 5401–5448, doi:10.1002/2013JA019748.
- Liemohn, M. W., J. U. Kozyra, V. K. Jordanova, G. V. Khazanov, M. F. Thomsen, and T. E. Cayton (1999), Analysis of early phase ring current recovery mechanisms during geomagnetic storms, *Geophys. Res. Lett.*, *26*, 2845–2848, doi:10.1029/1999GL900611.
- Lindsay, G. M., C. T. Russell, and J. G. Luhmann (1995), Coronal mass ejection and stream interaction region characteristics and their potential geomagnetic effectiveness, *J. Geophys. Res.*, *100*, 16,999–17,014, doi:10.1029/95JA00525.
- Lomb, N. R. (1976), Least-squares frequency analysis of unequally spaced data, *Astrophys. Space Sci.*, *39*, 447–462, doi:10.1007/BF00648343.
- Malandraki, O. E., E. T. Sarris, L. J. Lanzerotti, P. Trochoutsos, G. Tsiropoula, and M. Pick (2002), Solar energetic particles inside a coronal mass ejection event observed with the ACE spacecraft, *J. Atmos. Sol. Terr. Phys.*, *64*, 517–525, doi:10.1016/S1364-6826(02)00008-1.
- Marubashi, K. (1986), Structure of the interplanetary magnetic clouds and their solar origins, *Adv. Space Res.*, *6*, 335–338, doi:10.1016/0273-1177(86)90172-9.
- Marubashi, K. (2000), Physics of interplanetary magnetic flux ropes: Toward prediction of geomagnetic storms, *Adv. Space Res.*, *26*, 55–66, doi:10.1016/S0273-1177(99)01026-1.
- Marubashi, K., and R. P. Lepping (2007), Long-duration magnetic clouds: A comparison of analyses using torus- and cylinder-shaped flux rope models, *Ann. Geophys.*, *25*, 2453–2477, doi:10.5194/angeo-25-2453-2007.
- Marubashi, K., S. Akiyama, S. Yashiro, N. Gopalswamy, K.-S. Cho, and Y.-D. Park (2015), Geometrical relationship between interplanetary flux ropes and their solar sources, *Sol. Phys.*, *290*, 1371–1397, doi:10.1007/s11207-015-0681-4.
- McComas, D. J., J. T. Gosling, S. J. Bame, E. J. Smith, and H. V. Cane (1989), A test of magnetic field draping induced Bz perturbations ahead of fast coronal mass ejecta, *J. Geophys. Res.*, *94*, 1465–1471, doi:10.1029/JA094iA02p01465.
- McIntosh, S. W., R. J. Leamon, and B. De Pontieu (2011), The spectroscopic footprint of the fast solar wind, *Astrophys. J.*, *727*, 7, doi:10.1088/0004-637X/727/1/7.

- Moran, P. J., S. Ananthakrishnan, V. Balasubramanian, A. R. Breen, A. Canals, R. A. Fallows, P. Janardhan, M. Tokumaru, and P. J. S. Williams (2000), Observations of interplanetary scintillation during the 1998 whole Sun month: A comparison between EISCAT, ORT and Nagoya data, *Ann. Geophys.*, *18*, 1003–1008, doi:10.1007/s00585-000-1003-0.
- Neugebauer, M., et al. (1998), Spatial structure of the solar wind and comparisons with solar data and models, *J. Geophys. Res.*, *103*, 14,587–14,600, doi:10.1029/98JA00798.
- Owens, M., and P. Cargill (2004), Non-radial solar wind flows induced by the motion of interplanetary coronal mass ejections, *Ann. Geophys.*, *22*, 4397–4406, doi:10.5194/angeo-22-4397-2004.
- Posch, J. L., M. J. Engebretson, V. A. Pilipenko, W. J. Hughes, C. T. Russell, and L. J. Lanzerotti (2003), Characterizing the long-period ULF response to magnetic storms, *J. Geophys. Res.*, *108*, 1029, doi:10.1029/2002JA009386.
- Rastogi, R. G., P. Janardhan, K. Ahmed, A. C. Das, and S. K. Bisoi (2010), Unique observations of a geomagnetic  $SI^+$ – $SI^-$  pair: Solar sources and associated solar wind fluctuations, *J. Geophys. Res.*, *115*, A12110, doi:10.1029/2010JA015708.
- Rosenberg, R. L., and P. J. Coleman Jr. (1980), Solar cycle-dependent north-south field configurations observed in solar wind interaction regions, *J. Geophys. Res. Space Physics*, *85*, 3021–3032, doi:10.1029/JA085iA06p03021.
- Russell, C. T., M. Ginskey, and S. M. Petrincic (1994), Sudden impulses at low latitude stations: Steady state response for southward interplanetary magnetic field, *J. Geophys. Res.*, *99*, 13,403–13,408, doi:10.1029/94JA00549.
- Scargle, J. D. (1982), Studies in astronomical time series analysis. II—Statistical aspects of spectral analysis of unevenly spaced data, *Astrophys. J.*, *263*, 835–853, doi:10.1086/160554.
- Scargle, J. D. (1989), Studies in astronomical time series analysis. III—Fourier transforms, autocorrelation functions, and cross-correlation functions of unevenly spaced data, *Astrophys. J.*, *343*, 874–887, doi:10.1086/167757.
- Scherrer, P. H., et al. (1995), The solar oscillations investigation—Michelson Doppler imager, *Sol. Phys.*, *162*, 129–188, doi:10.1007/BF00733429.
- Sheeley, N. R., Jr., J. W. Harvey, and W. C. Feldman (1976), Coronal holes, solar wind streams, and recurrent geomagnetic disturbances – 1973–1976, *Sol. Phys.*, *49*, 271–278, doi:10.1007/BF00162451.
- Siegel, A. F. (1980), Testing for periodicity in a time series, *Am. Statist. Assoc.*, *75*, 345–348.
- Skoug, R. M., et al. (1999), A prolonged  $He^+$  enhancement within a coronal mass ejection in the solar wind, *Geophys. Res. Lett.*, *26*, 161–164, doi:10.1029/1998GL900207.
- Smith, E. J., and J. H. Wolfe (1976), Observations of interaction regions and corotating shocks between one and five AU—Pioneers 10 and 11, *Geophys. Res. Lett.*, *3*, 137–140, doi:10.1029/GL003i003p00137.
- Smith, J. P., M. F. Thomsen, J. E. Borovsky, and M. Collier (1999), Solar wind density as a driver for the ring current in mild storms, *Geophys. Res. Lett.*, *26*, 1797–1800, doi:10.1029/1999GL900341.
- Sonett, C. P., and D. S. Colburn (1965), The  $SI^+$ – $SI^-$  pair and interplanetary forward-reverse shock ensembles, *Planet. Space Sci.*, *13*, 675–692, doi:10.1016/0032-0633(65)90046-2.
- Stone, E. C., A. M. Frandsen, R. A. Mewaldt, E. R. Christian, D. Margolies, J. F. Ormes, and F. Snow (1998), The Advanced Composition Explorer, *Space Sci. Rev.*, *86*, 1–22, doi:10.1023/A:1005082526237.
- Tang, F., S.-I. Akasofu, E. Smith, and B. Tsurutani (1985), Magnetic fields on the Sun and the north-south component of transient variations of the interplanetary magnetic field at 1 AU, *J. Geophys. Res.*, *90*, 2703–2712, doi:10.1029/JA090iA03p02703.
- Tang, F., B. T. Tsurutani, E. J. Smith, W. D. Gonzalez, and S. I. Akasofu (1989), Solar sources of interplanetary southward  $B_z$  events responsible for major magnetic storms (1978–1979), *J. Geophys. Res. Space Physics*, *94*, 3535–3541, doi:10.1029/JA094iA04p03535.
- Tanskanen, E. I., J. A. Slavin, D. H. Fairfield, D. G. Sibeck, J. Gjerloev, T. Mukai, A. Ieda, and T. Nagai (2005), Magnetotail response to prolonged southward IMF  $B_z$  intervals: Loading, unloading, and continuous magnetospheric dissipation, *J. Geophys. Res.*, *110*, A03216, doi:10.1029/2004JA010561.
- Terasawa, T., et al. (1997), Solar wind control of density and temperature in the near-Earth plasma sheet: WIND/GEOTAIL collaboration, *Geophys. Res. Lett.*, *24*, 935–938, doi:10.1029/96GL04018.
- Thompson, B. J., E. W. Cliver, N. Nitta, C. Delannée, and J.-P. Delaboudinière (2000), Coronal dimmings and energetic CMEs in April–May 1998, *Geophys. Res. Lett.*, *27*, 1431–1434, doi:10.1029/1999GL003668.
- Thomsen, M. F., J. E. Borovsky, D. J. McComas, and M. R. Collier (1998), Variability of the ring current source population, *Geophys. Res. Lett.*, *25*, 3481–3484, doi:10.1029/98GL02633.
- Tsurutani, B. T., and C.-I. Meng (1972), Interplanetary magnetic-field variations and substorm activity, *J. Geophys. Res.*, *77*, 2964–2970, doi:10.1029/JA077i016p02964.
- Tsurutani, B. T., C. T. Russell, J. H. King, R. D. Zwickl, and R. P. Lin (1984), A kinky heliospheric current sheet—Cause of CDAW-6 substorms, *Geophys. Res. Lett.*, *11*, 339–342, doi:10.1029/GL011i004p00339.
- Tsurutani, B. T., E. J. Smith, W. D. Gonzalez, F. Tang, and S. I. Akasofu (1988), Origin of interplanetary southward magnetic fields responsible for major magnetic storms near solar maximum (1978–1979), *J. Geophys. Res.*, *93*, 8519–8531, doi:10.1029/JA093iA08p08519.
- Tsurutani, B. T., W. D. Gonzalez, F. Tang, and Y. T. Lee (1992), Great magnetic storms, *Geophys. Res. Lett.*, *19*, 73–76, doi:10.1029/91GL02783.
- Tsurutani, B. T., C. M. Ho, J. K. Arballo, B. E. Goldstein, and A. Balogh (1995), Large amplitude IMF fluctuations in corotating interaction regions: Ulysses at midlatitudes, *Geophys. Res. Lett.*, *22*, 3397–3400, doi:10.1029/95GL03179.
- Tsurutani, B. T., et al. (1998), The January 10, 1997 auroral hot spot, horseshoe aurora and first substorm: A CME loop? *Geophys. Res. Lett.*, *25*, 3047–3050, doi:10.1029/98GL01304.
- Tsurutani, B. T., et al. (2006), Corotating solar wind streams and recurrent geomagnetic activity: A review, *J. Geophys. Res.*, *111*, A07S01, doi:10.1029/2005JA011273.
- Tsurutani, B. T., G. S. Lakhina, O. P. Verkhoglyadova, W. D. Gonzalez, E. Echer, and F. L. Guarnieri (2011), A review of interplanetary discontinuities and their geomagnetic effects, *J. Atmos. Sol. Terr. Phys.*, *73*, 5–19, doi:10.1016/j.jastp.2010.04.001.
- Tsurutani, B. T., E. Echer, K. Shibata, O. P. Verkhoglyadova, A. J. Mannucci, W. D. Gonzalez, J. U. Kozyra, and M. Pätzold (2014), The interplanetary causes of geomagnetic activity during the 7–17 March 2012 interval: A CAWSES II overview, *J. Weather Space Clim.*, *4*(27), A02, doi:10.1051/swsc/2013056.
- Tsurutani, B. T., R. Hajra, E. Echer, and J. W. Gjerloev (2015), Extremely intense ( $SML < -2500$  nT) substorms: Isolated events that are externally triggered?, *Ann. Geophys.*, *33*, 519–524, doi:10.5194/angeo-33-519-2015.
- Viall, N. M., and A. Vourlidas (2015), Periodic density structures and the origin of the slow solar wind, *Astrophys. J.*, *807*, 176, doi:10.1088/0004-637X/807/2/176.
- Viall, N. M., L. Kepko, and H. E. Spence (2008), Inherent length-scales of periodic solar wind number density structures, *J. Geophys. Res.*, *113*, A07101, doi:10.1029/2007JA012881.
- Viall, N. M., L. Kepko, and H. E. Spence (2009a), Relative occurrence rates and connection of discrete frequency oscillations in the solar wind density and dayside magnetosphere, *J. Geophys. Res.*, *114*, A01201, doi:10.1029/2008JA013334.

- Viall, N. M., H. E. Spence, and J. Kasper (2009b), Are periodic solar wind number density structures formed in the solar corona?, *Geophys. Res. Lett.*, *36*, L23102, doi:10.1029/2009GL041191.
- Viall, N. M., H. E. Spence, A. Vourlidas, and R. Howard (2010), Examining periodic solar-wind density structures observed in the SECCHI heliospheric imagers, *Sol. Phys.*, *267*, 175–202, doi:10.1007/s11207-010-9633-1.
- Villante, U., and M. Piersanti (2009), Analysis of geomagnetic sudden impulses at low latitudes, *J. Geophys. Res.*, *114*, A06209, doi:10.1029/2008JA013920.
- Villante, U., M. Piersanti, P. di Giuseppe, M. Villante, T. L. Zhang, and W. Magnes (2005), Sudden commencement event of 17 April 2002: Aspects of the geomagnetic response at low latitudes, *J. Geophys. Res.*, *110*, A12523, doi:10.1029/2004JA010978.
- Walker, R. J., M. Ashour-Abdalla, M. El Alaoui, and F. V. Coroniti (2006), Magnetospheric convection during prolonged intervals with southward interplanetary magnetic field, *J. Geophys. Res.*, *111*, A10219, doi:10.1029/2005JA011541.
- Wang, C. B., J. K. Chao, and C.-H. Lin (2003), Influence of the solar wind dynamic pressure on the decay and injection of the ring current, *J. Geophys. Res.*, *108*, 1341, doi:10.1029/2003JA009851.
- Wang, H., P. R. Goode, C. Denker, G. Yang, V. Yurchishin, N. Nitta, J. B. Gurman, C. St. Cyr, and A. G. Kosovichev (2000), Comparison of the 1998 April 29 *M6.8* and 1998 November 5 *M8.4* flares, *Astrophys. J.*, *536*, 971–981, doi:10.1086/308964.
- Wang, T., Y. Yan, J. Wang, H. Kurokawa, and K. Shibata (2002), The large-scale coronal field structure and source region features for a halo coronal mass ejection, *Astrophys. J.*, *572*, 580–597, doi:10.1086/340189.
- Webb, D. F., and A. J. Hundhausen (1987), Activity associated with the solar origin of coronal mass ejections, *Sol. Phys.*, *108*, 383–401, doi:10.1007/BF00214170.
- Wilson, C. R., and M. Sugiura (1961), Hydromagnetic interpretation of sudden commencements of magnetic storms, *J. Geophys. Res.*, *66*, 4097–4111, doi:10.1029/JZ066i012p04097.
- Yumoto, K., and CPMN Group (2001), Characteristics of Pi 2 magnetic pulsations observed at the CPMN stations: A review of the STEP results, *Earth Planets Space*, *53*, 981–992.
- Zhang, X.-Y., and M. B. Moldwin (2014), The source, statistical properties, and geoeffectiveness of long-duration southward interplanetary magnetic field intervals, *J. Geophys. Res. Space Physics*, *119*, 658–669, doi:10.1002/2013JA018937.
- Zhao, X. P., and J. T. Hoeksema (1998), Central axial field direction in magnetic clouds and its relation to southward interplanetary magnetic field events and dependence on disappearing solar filaments, *J. Geophys. Res.*, *103*, 2077, doi:10.1029/97JA03234.
- Zhou, X., and B. T. Tsurutani (2001), Interplanetary shock triggering of nightside geomagnetic activity: Substorms, pseudobreakups, and quiescent events, *J. Geophys. Res.*, *106*, 18,957–18,968, doi:10.1029/2000JA003028.